

# Optimal Transport-Based Generative Models for Bayesian Posterior Sampling

Ke Li<sup>1</sup>, Wei Han<sup>1</sup>, Yuexi Wang<sup>1</sup>, and Yun Yang<sup>2</sup>

<sup>1</sup>Department of Statistics, University of Illinois Urbana-Champaign, USA

<sup>2</sup>Department of Mathematics, University of Maryland, College Park, USA

April 14, 2025

## Abstract

We investigate the problem of sampling from posterior distributions with intractable normalizing constants in Bayesian inference. Our solution is a new generative modeling approach based on optimal transport (OT) that learns a deterministic map from a reference distribution to the target posterior through constrained optimization. The method uses structural constraints from OT theory to ensure uniqueness of the solution and allows efficient generation of many independent, high-quality posterior samples. The framework supports both continuous and mixed discrete-continuous parameter spaces, with specific adaptations for latent variable models and near-Gaussian posteriors. Beyond computational benefits, it also enables new inferential tools based on OT-derived multivariate ranks and quantiles for Bayesian exploratory analysis and visualization. We demonstrate the effectiveness of our approach through multiple simulation studies and a real-world data analysis.

*Keywords:* Bayesian Inference, Generative Models, Latent Variable Models, Multivariate Quantiles, Optimal Transport, Posterior Sampling.

## 1 Introduction

A central problem in modern Bayesian statistics is how to conduct valid statistical inference on model parameters in a computationally efficient manner. In a standard Bayesian model, all information about model parameter  $\theta$  in the parameter space  $\Theta \subset \mathbb{R}^p$  is summarized in the posterior distribution

$$\pi_n(\theta) := p(\theta | Z^{(n)}) = \frac{\pi(\theta) p(Z^{(n)} | \theta)}{\int_{\Theta} \pi(\theta) p(Z^{(n)} | \theta) d\theta}, \quad \forall \theta \in \Theta \quad (1)$$

obtained by applying the Bayes rule, where  $\pi(\theta)$  denotes the prior distribution (density function) over  $\Theta$ ,  $Z^{(n)} = (Z_1, Z_2, \dots, Z_n)$  is a sample of  $n$  observations, and  $p(Z^{(n)} | \theta)$  represents the likelihood function specified by the statistical model.

The main hurdle in implementing Bayesian inference is the multi-dimensional integral as the normalization constant appearing in equation (1), i.e., the marginal data density  $p(Z^n) = \int_{\Theta} \pi(\theta) p(Z^{(n)} | \theta) d\theta$ . This integral is often mathematically intractable unless a conjugate prior is employed, which however significantly restricts the applicability of the Bayesian procedure to complicated models where a conjugate prior is either difficult to identify or not flexible enough to use.

To circumvent this issue, two approaches are widely used to enable Bayesian inference without explicit knowledge of the normalizing constant. The first approach is Markov Chain Monte Carlo (MCMC, Gelman et al., 2013), which generates approximate posterior samples by constructing a Markov chain whose equilibrium distribution matches the target. The second approach employs variational approximation (Blei et al., 2017), which reformulates the integration problem as an optimization problem. Yet, both approaches have notable limitations. MCMC algorithms often suffer from slow mixing, especially in high-dimensional or highly structured models, leading to high correlation among successive draws. On the other hand, while variational approximation scales well to large datasets, it does not guarantee exact sampling from the target density, potentially resulting in biased estimation and unreliable uncertainty quantification.

This paper introduces a novel sampling framework that combines generative modeling with optimal transport theory. Our approach eliminates the need for Markov chain simulation while producing *independent and nearly exact* samples from the target distribution, achieving computational efficiency comparable to variational approximations. The method works by learning a (potentially nonlinear) rank-preserving (c.f. Section 4.3) transport map  $T^*$  that transforms i.i.d. samples from a simple reference distribution  $\mu$  (such as a standard Gaussian or the prior  $\pi$ ) into samples from the target distribution  $\pi_n$ . Formally, this corresponds to  $\pi_n$  being the pushforward distribution  $[T^*]_{\#}\mu$  of  $\mu$  under  $T^*$ . We formulate  $T^*$  as the unique solution to an optimization problem, guaranteeing both scalability and computational tractability. Once obtained,  $T^*$  enables efficient generation of an arbitrary number of independent posterior draws.

The idea of using transport maps for posterior sampling first appeared in El Moselhy and Marzouk (2012) and has since been explored in several works, including Hoffman et al. (2019); Duan (2021); Katzfuss and Schäfer (2021). However, our approach differs from prior work through its explicit structural constraints on the class of transport maps to ensure identifiability. Previous approaches lacked such constraints, often resulting in non-unique transport maps that lead to computational instability and inefficiency. In contrast, we constrain  $T^*$  to be the Optimal Transport (OT) map from the reference distribution  $\mu$  to the posterior  $\pi_n$  in the Monge problem (Santambrogio, 2015; Villani, 2008), specifically requiring that  $T^*$  minimizes the  $\ell_2$  transportation cost, that is,

$$T^* = \arg \min_{T \in \mathcal{T}} \mathbb{E}_{X \sim \mu} [\|T(X) - X\|_2^2], \quad (2)$$

where  $\mathcal{T} = \{T : \pi_n = T_{\#}\mu\}$  is the class of all transport maps that pushforward the reference distribution  $\mu$  to target distribution  $\pi_n$ . From a modeling perspective, this constraint produces the *most parsimonious* map that transports  $\mu$  to  $\pi_n$  up to a measure-preserving transformation (see Remark 2 and Brenier (1991)). From a practical perspective, the estimated transport map is *more interpretable*. For example, the collection of transportation maps  $\{[(1-t)id + tT^*]_{\#}\mu : t \in [0, 1]\}$ , where  $id$  denotes the identity map, describes the shortest — or geodesic — path connecting the prior  $\pi$  and posterior  $\pi_n$  in the space of all probability distributions. In particular, the 2-Wasserstein distance  $W_2(\pi, \pi_n)$ , which quantifies the discrepancy between the prior and posterior and reflects the amount of information contributed by the data, can be efficiently computed as  $\{\mathbb{E}_{\theta \sim \pi} [\|T^*(\theta) - \theta\|_2^2]\}^{1/2}$ , since  $T^*$  provides the optimal transport map. Moreover, once  $T^*$  is available, it enables new posterior summaries and inference through the computation of OT-derived multivariate ranks, as well as the construction of center-outward quantile contours and sign curves as proposed by Hallin et al. (2021) (see Section 4.3), providing powerful new tools for Bayesian exploratory analysis and visualization.

Unfortunately, directly computing the optimal transport map  $T^*$  from definition (2) is intractable in a Bayesian setting, primarily because the constraint  $\pi_n = T_{\#}\mu$  is difficult to enforce analytically

or computationally. As an alternative, we consider the following variational formulation:

$$\min_{T \in \mathcal{T}} d_{\text{KL}}(T_{\#}\mu \parallel \pi_n), \quad (3)$$

where  $\mathcal{T}$  is a pre-specified class of transport maps that satisfies certain structural conditions derived from optimal transport theory, ensuring that  $T^*$  is the unique solution. Here,  $d_{\text{KL}}(p \parallel q)$  denotes the Kullback–Leibler (KL) divergence between two generic distributions  $p$  and  $q$ . This new formulation offers several key advantages.

First, the class  $\mathcal{T}$  is independent of the target distribution  $\pi_n$  and is derived purely from a primal-dual analysis of the OT problem (2). This structural independence provides both theoretical clarity and practical convenience. For instance, in the setting where  $\theta$  contains only continuous variables (Section 3.1),  $\mathcal{T}$  can be taken as the set of gradients of all convex functions. In this setting, the inverse map  $(T^*)^{-1}$  can be efficiently computed by solving a convex optimization problem, which is particularly useful for constructing center-outward ranks (see Section 4.3). Additionally, when  $\theta$  is mixed — i.e., it contains both continuous and discrete components as is common in Bayesian latent variable models —  $\mathcal{T}$  admits a more intricate but still analytically tractable characterization (c.f. Theorem 1 in Section 3.2). Second, in the same spirit as variational inference (Blei et al., 2017), minimizing the KL divergence in the objective functional avoids the need to compute the unknown normalization constant  $p(Z^n)$ . Moreover, an equivalent formulation of (3) exists that does not require explicitly evaluating the probability density function of  $T_{\#}\mu$ , by leveraging the invariance of KL divergence under invertible transformations (c.f. Lemma 1). Fortunately, the structural conditions imposed on  $\mathcal{T}$  ensure that any  $T \in \mathcal{T}$  is invertible, and therefore, the equivalent formulation remains valid along any optimization trajectory within  $\mathcal{T}$  when solving the original problem (3).

In this work, we further adapt the characterization of the optimal transport (OT) map  $T^*$  from classical optimal transport theory to the Bayesian inference setting in several key ways. First, we provide explicit characterizations of  $T^*$  in settings where  $\theta$  includes both continuous and discrete components, as in Bayesian latent variable models. Our formulation extends the classical semi-discrete OT framework — where one distribution is fully discrete — to the more general

mixed discrete-continuous case, which, to our knowledge, has not been previously addressed in the literature. Second, for regular parametric models with approximately Gaussian posteriors, we show that restricting the transport map class  $\mathcal{T}$  to a subset of affine transformations is sufficient to preserve approximation quality up to the statistical accuracy of the problem, while significantly reducing computational complexity. Finally, to further enhance scalability in Bayesian latent variable models, we incorporate the mean-field approximation technique (Blei et al., 2017; Zhang and Yang, 2024) from variational inference to impose additional structure on  $\mathcal{T}$ , further reducing its computational complexity while maintaining modeling flexibility and statistical accuracy.

The remainder of the paper is organized as follows. Section 2 provides a general overview of generative model learning and key theoretical results in optimal transport that form the foundation of our approach. In Section 3, we introduce our methodology for both continuous and mixed parameter distributions. Section 4 presents three applications of our method: the first two involve specialized approximation classes, while the third highlights the inferential capabilities enabled by our framework. We evaluate the performance of our method against existing transport map approaches using simulated examples in Section 5, and conduct a real-data analysis of the *yeast* dataset in Section 6. Finally, we conclude with a discussion of future research directions in Section 7.

**Notation.** We write  $\text{spt}(P)$  to denote the support of a probability distribution  $P$ . The inner product  $\langle \cdot, \cdot \rangle$  is defined by  $\langle a, b \rangle = \sum_{i=1}^d a_i b_i$  for vectors  $a, b \in \mathbb{R}^d$ . The abbreviation i.i.d. stands for “independently and identically distributed”. We denote the local Hölder space of smoothness level  $k + \beta$  over a bounded open set  $A \subset \mathbb{R}^p$  by  $C_{\text{loc}}^{k,\beta}(A)$ , where  $\beta \in (0, 1)$  and  $k$  is a nonnegative integer. That is,  $u \in C_{\text{loc}}^{k,\beta}(A)$  if, for every compact subset  $V \subset A$ , we have  $u \in C^{k,\beta}(V)$ . The effective domain of a function  $u$  (often referred to simply as its domain) is defined as  $\text{Dom}(u) := \{x \in \mathbb{R}^p \mid |u(x)| < \infty\}$ . The closure of a set  $\Omega$  is denoted by  $\bar{\Omega}$ .

## 2 Background on Generative Models and Optimal Transport

In this section, we begin by introducing the concept of generative models and discuss how they can be adapted for posterior approximation. We then provide a brief overview of optimal transport theory and present the formal definition of the optimal transport map.

## 2.1 Generative model approaches for Bayesian sampling

In the machine learning literature, generative models, such as Generative Adversarial Network (GAN, Goodfellow et al. (2014); Li et al. (2015); Biau et al. (2020)), Wasserstein GAN (WGAN, Arjovsky et al. (2017)) and Wasserstein Auto-Encoder (WAE, Tolstikhin et al. (2019); Zhao et al. (2018)), have received great success in generating synthetic realistic-looking images and texts (Brock et al., 2018; van den Oord et al., 2016) by implicit distribution estimation over complex data space bypassing the need of evaluating probability densities. Generative model based approaches for statistical inference (Mohamed and Lakshminarayanan, 2016; Huszár, 2017) avoid explicitly specifying the likelihood function while utilizing the expressive power of neural networks to capture underlying probabilistic structures. In our setting of posterior sampling, the generative model operates over the parameter space  $\Theta \subset \mathbb{R}^p$ , which may also include latent variables.

A *generative model* is formally defined as a pair  $(\mu, T)$ , where  $\mu$  is a distribution on a latent space  $\mathcal{X} \subset \mathbb{R}^p$ , referred to as the reference or generative distribution, and  $T : \mathcal{X} \rightarrow \Theta$  is a map from the latent space to the data space  $\Theta$ , known as the transport map or generative map. Ideally, if  $X \sim \mu$ , then  $T(X) \sim \nu$ , where  $\nu$  denotes the target distribution we aim to approximate. In other words, the target distribution  $\nu$  can be represented via the generative model  $(\mu, T)$  through the pushforward measure  $\nu = T_{\#}\mu$ . The set  $\mathcal{D}_{\mathcal{T}} = \{T_{\#}\mu : T \in \mathcal{T}\}$ , where  $\mathcal{T}$  is a class of transport maps from  $\mathcal{X}$  to  $\Theta$ , defines the associated *generator class*. In practice, the reference distribution  $\mu$  is typically chosen to be a simple, tractable distribution such as a standard Gaussian or uniform distribution, from which samples can be easily drawn. Given a generative model  $(\mu, T)$ , samples from the pushforward distribution  $T_{\#}\mu$  are readily obtained by drawing i.i.d. samples  $X_i \sim \mu$  and computing  $T(X_i)$ . In the Bayesian setting, it is natural to take the prior distribution  $\pi$  as the reference distribution; furthermore, when the prior depends on hyperparameters, the generator class can be extended to  $\mathcal{D}_{\Upsilon, \mathcal{T}} = \{T_{\#}\mu : \mu \in \Upsilon; T \in \mathcal{T}\}$ , where  $\Upsilon$  denotes a family of reference distributions parameterized by those hyperparameters.

Generative model learning refers to the problem of finding a transport map  $T^* \in \mathcal{T}$  such that its pushforward measure  $[T^*]_{\#}\mu$  is as close as possible to a target distribution  $\nu^*$  under a chosen discrepancy metric  $d_{\mathcal{G}}$ . Formally, this corresponds to solving the optimization problem of

$T^* = \arg \min_{T \in \mathcal{T}} d_G(T_{\#}\mu, \nu^*)$ . In the typical setting of learning a distribution over complex data types such as images or text, one only has access to a finite number  $n$  of i.i.d. samples  $\{Z_1, Z_2, \dots, Z_n\}$  from the unknown distribution  $\nu^*$ . In such cases, a convenient choice of discrepancy metric is the *adversarial risk*, defined as  $d_G(\nu_1, \nu_2) = \sup_{f \in \mathcal{F}} |\mathbb{E}_{\nu_1}[f(Z)] - \mathbb{E}_{\nu_2}[f(Z)]|$ , where  $\mathcal{F}$  is a class of discriminator functions. This choice is particularly appealing because the term  $\mathbb{E}_{\nu^*}[f(Z)]$  can be approximated by the empirical average  $n^{-1} \sum_{i=1}^n f(Z_i)$ , making the objective computationally tractable. This framework underlies the training of GANs (Goodfellow et al., 2014; Li et al., 2015; Biau et al., 2020).

In this paper, we adapt generative model learning to the Bayesian framework. Our objective is to generate independent samples from the posterior distribution  $\pi_n$ , which is only known up to a normalizing constant. Throughout the paper, we use the terms “target distribution” and “posterior distribution” interchangeably. Due to the intractability of the normalizing constant, the adversarial risk is no longer a suitable choice for the discrepancy metric  $d_G$ . Instead, inspired by variational inference (Blei et al., 2017), we adopt the Kullback–Leibler (KL) divergence as our discrepancy metric. The KL divergence allows for optimization without requiring explicit knowledge of the normalization constant, making it particularly well-suited for Bayesian settings. In particular, we consider the following optimization problem for Bayesian transport map learning with a fixed reference distribution  $\mu$

$$\min_{T \in \mathcal{T}} d_{\text{KL}}(T_{\#}\mu \parallel \pi_n), \quad (4)$$

where the transport map class  $\mathcal{T}$  is a flexible function space (c.f. Section 3.1 and Section 3.2 for its choice). However, unlike variational inference, directly solving (4) is generally computationally infeasible, as evaluating the KL divergence requires an explicit expression for the density of the pushforward distribution  $T_{\#}\mu$ . This, in turn, typically necessitates knowledge of the inverse map  $T^{-1}$  — if it even exists or is tractable to compute. Fortunately, the KL divergence in (4) is invariant under common invertible transformations applied to both  $\mu$  and  $\pi_n$ . Leveraging this key property, we reformulate the original optimization problem into an equivalent form that avoids computing  $T^{-1}$ , as formalized in the following lemma. The proof follows from a standard change-of-variables

argument and is provided in Section C.2.

**Lemma 1.** *Assume that each element  $T \in \mathcal{T}$  is differentiable and invertible on the support of  $\mu$ . Then optimization problem in (4) is equivalent to*

$$\max_{T \in \mathcal{T}} \mathbb{E}_\mu [\log(\pi_n \circ T) + \log |\det(J_T)|]. \quad (5)$$

where  $J_T \in \mathbb{R}^{p \times p}$  denotes the Jacobian matrix associated with map  $T$  from  $\mathbb{R}^p$  to  $\mathbb{R}^p$  and  $\det(A)$  denotes the determinant of a square matrix  $A$ .

Lemma 1 enables us to identify the optimal transport map  $T^*$  without computing the intractable normalization constant. Moreover, it offers an intuitive interpretation of the objective function in (5). The first term,  $\log(\pi_n \circ T)$ , can be viewed as a goodness-of-fit term that encourages alignment with the target distribution  $\pi_n$ , while the second term acts as a regularization term that penalizes the “roughness” of the transport map  $T$ . More specifically, for each  $X \sim \mu$  in the latent space, the term  $|\det(J_T(X))|$  quantifies the degree of local distortion induced by the Jacobian map  $J_T(X) : \mathbb{R}^p \rightarrow \mathbb{R}^p$  around the point  $X$ . As shown later via the Monge–Ampère equation (6) (see Lemma 2), the optimal transport map  $T^*$  satisfies  $|\det(J_{T^*})| = \frac{\mu}{\pi_n \circ T^*}$ . Substituting this into the objective in (5) reveals that its optimal value corresponds to the negative differential entropy of the reference distribution  $\mu$ , given by  $-h(\mu) = \mathbb{E}_\mu[\log \mu]$ .

## 2.2 Review of optimal transport theory

Optimal transport (OT), or transportation theory, originates from the study by French mathematician Gaspard Monge in 1781, and has recently been found useful in solving a number of machine learning problems including generative model learning. We refer the reader to two books, one by Villani (2008) and the other by Santambrogio (2015), for a comprehensive and thorough discussion of theoretical developments of OT. In this subsection, we briefly review some theoretical background and fundamental results of OT that are necessary before introducing our development.

We focus on the OT problem with quadratic cost, commonly known as the Kantorovich Problem

(KP), defined as

$$(KP) \quad \inf_{\gamma \in \Pi(\nu_1, \nu_2)} \int \|x - y\|^2 d\gamma(x, y)$$

where  $\Pi(\nu_1, \nu_2)$  is the set of all couplings between two probability distributions,  $\nu_1$  over  $\mathcal{X} \subset \mathbb{R}^p$  and  $\nu_2$  over  $\mathcal{Y} \subset \mathbb{R}^p$ . That is,  $\gamma \in \Pi(\nu_1, \nu_2)$  if and only if its marginal distributions are  $\nu_1$  and  $\nu_2$ , respectively.

The Kantorovich problem always admits a solution (Santambrogio, 2015, Theorem 1.7), referred as the *optimal transport plan*. The optimal objective value of KP is defined as the squared 2-Wasserstein distance between  $\nu_1$  and  $\nu_2$ , denoted as  $W_2^2(\nu_1, \nu_2)$ . In particular, when one of the distributions, say  $\nu_1$ , is absolutely continuous with respect to the Lebesgue measure on  $\mathbb{R}^p$ , the first part of the lemma below (Santambrogio, 2015, Theorem 1.22) shows that, under some mild conditions, the optimal transport plan is unique and takes the form of  $(id, T^*)_{\#}\nu_1$ , implying  $\nu_2 = T^*_{\#}\nu_1$  (also see, e.g., Brenier, 1991; McCann, 1995).

**Lemma 2** (Optimal transport solution existence and regularity). *Suppose  $\nu_1$  and  $\nu_2$  both have finite second moments, and  $\nu_1$  gives no mass to  $(p - 1)$  surfaces of class  $C^2$ , then we have:*

1. *An optimal transport plan solving (KP) exists and is unique. It admits the form of  $(id, T^*)_{\#}\nu_1$  with  $T^* = \nabla u^*$ , where  $u^*$  is a convex function. The converse is also true: if there exists a convex function  $u$  such that  $[\nabla u^*]_{\#}\nu_1 = \nu_2$ , then  $(id, T^*)_{\#}\nu_1$  with  $T^* = \nabla u^*$  is the unique solution of (KP). The function  $u^*$  is referred as the optimal potential function.*
2. *(Santambrogio, 2015, Section 1.7.6.) If both  $\nu_1$  and  $\nu_2$  are absolutely continuous with respect to the Lebesgue measure of  $\mathbb{R}^p$ , with density functions denoted by  $\nu_1$  and  $\nu_2$  as well, then  $T^*$  is differentiable  $\nu_1$ -a.e., and solves the following Monge-Ampere equation:*

$$|\det(J_{T^*})| = \frac{\nu_1}{\nu_2 \circ T^*}, \quad \mu\text{-a.e.} \quad (6)$$

3. *Assume that  $\nu_1$  and  $\nu_2$  are supported on bounded open sets  $S_1$  and  $S_2$  in  $\mathbb{R}^d$  respectively, with  $S_2$  being convex. Then the smoothness of  $T^*$  is always one degree higher than the density*

functions, in the sense that if  $\mu \in C_{loc}^{k,\beta}(S_1)$  and  $\pi_n \in C_{loc}^{k,\beta}(S_2)$ , then  $T^* \in C_{loc}^{k+1,\beta}(S_1)$ . This regularity extends to the closure  $\bar{S}_1$  and  $\bar{S}_2$ .

The regularity results on the smoothness of  $T$  in the lemma follows from Caffarelli’s regularity theory (Villani, 2003; Caffarelli, 1992a,b). Various versions of this result are available, and we present the sufficient condition from De Philippis and Figalli (2014, Theorem 3.1–3.3).

Another commonly used formulation of the optimal transport is the Monge problem (MP), which seeks a transport map  $T^*$  that minimizes the expected quadratic transportation cost while exactly pushing forward  $\nu_1$  to  $\nu_2$ :

$$(MP) \quad \inf_T \int \|x - T(x)\|^2 d\nu_1(x), \quad \text{s.t.} \quad T_{\#}\nu_1 = \nu_2.$$

Under the regularity conditions stated in Lemma 2, problem (MP) admits a unique solution, referred to as the *optimal transport map*. However, it is important to note that (MP) may have no solution if these regularity conditions are not satisfied; see, for example, Section 1.4 in Santambrogio (2015). Moreover, if  $\nu_2$  assigns no mass to any  $(p - 1)$ -dimensional  $C^2$  surface, then the optimal transport map  $T^*$  is invertible, and there exists a unique convex function  $u^\dagger$  such that  $[\nabla u^\dagger]_{\#}\nu_2 = \nu_1$ . This function  $u^\dagger$  is related to the potential  $u^*$  through the relation  $\nabla u^\dagger = (\nabla u^*)^{-1}$ ,  $\mu$ -almost everywhere. We review this duality and the role of convex conjugates in Section C.1.

**Remark 1** (Multivariate extension of monotonicity). *In the one-dimensional case, the condition that a transport map  $T$  is the gradient of a convex function is equivalent to  $T$  being non-decreasing. In the multi-dimensional setting, the characterization of  $T$  as the gradient of a convex function generalizes this notion of monotonicity. Specifically, it ensures that a certain multivariate extension of quantiles (Chernozhukov et al., 2017) is well-defined (with the quantile ordering preserved through the mapping), and the transportation paths  $\gamma_x = (1 - t)x + t, T(x) ;, t \in [0, 1]$  are non-crossing for different  $x \in \mathcal{X}$  — a property known in optimal transport theory as the Monge–Mather shortening principle (Villani, 2008, Chapter 8). Leveraging this property, we show in Section 4.3 that when  $\mu$  is chosen to be the standard multivariate Gaussian distribution  $\mathcal{N}(0, I_p)$ , the center-outward ranks, quantile contours, and sign curves proposed by Hallin et al. (2021) can be constructed by mapping quantile spheres of  $\mathcal{N}(0, I_p)$  through the optimal transport map.*

**Remark 2** (OT map is the most parsimonious map). *Brenier’s polar factorization theorem (Brenier, 1991) states that any transport map  $T$  that pushforwards  $\nu_1$  to  $\nu_2$ , that is,  $\nu_2 = T_{\#}\nu_1$ , can be factorized as  $T = T^* \circ R$ , where  $T^*$  is the optimal transport map described in Lemma 2, and  $R$  is a measure-preserving map with respect to  $\nu_1$ , meaning  $R_{\#}\nu_1 = \nu_1$ . This decomposition highlights that the optimal transport map  $T^*$  is the most parsimonious way to transport  $\nu_1$  to  $\nu_2$ , corresponding to the special case where  $R = \text{id}$  is the identity map. While any transport map can be expressed as the composition of  $T^*$  with some measure-preserving map  $R$ , the converse does not necessarily hold, as  $R$  may not be invertible. Consequently, the optimal transport map can also be seen as the “minimal” transport map — analogous to the role of a minimal sufficient statistic in statistical inference — capturing only the essential transformation required to map  $\nu_1$  to  $\nu_2$ .*

Lemma 2 can be tailored to a special setting in which  $\nu_2$  is supported on a union of disjoint sets that are strongly separable — that is, each pair can be separated by a hyperplane. In this case, one can derive a more specialized characterization of the optimal potential function. For example, Kitagawa and McCann (2019, Theorem 5.1) show that when  $\text{spt}(\nu_2) = \overline{\Omega}_1 \cup \overline{\Omega}_2$ , where  $\Omega_k \subset \mathbb{R}^p$  ( $k = 1, 2$ ) are two disjoint convex subsets, the optimal convex potential  $u^*$  associated with the OT map  $T^*$  takes the form  $u^* = \max\{u_1^*, u_2^*\}$ . Here, each  $u_k^*$  is a convex function whose gradient  $\nabla u_k^*$  maps points to  $\overline{\Omega}_k$ , for  $k \in \{1, 2\}$ . Moreover, this result can be further generalized to the case where  $\text{spt}(\nu_2)$  consists of finitely many disjoint and strongly separable regions. Specifically, Kitagawa and McCann (2019, equation (5.5)) provide such an extension, which we summarize in the following lemma.

**Lemma 3** (Target distribution with disconnected support from Kitagawa and McCann (2019)). *Under the same conditions as in Lemma 2, and additionally assuming that  $\text{spt}(\nu_2) = \bigcup_{k \in I} \overline{\Omega}_k$  for a finite index set  $I$ , where each  $\overline{\Omega}_k$  can be separated from every other  $\overline{\Omega}_\ell$  ( $\ell \neq k$ ) by a hyperplane, the optimal potential function  $u^*$  associated with the OT map  $T^*$  from  $\nu_1$  to  $\nu_2$  can be expressed as*

$$u^*(x) = \max_{k \in I} u_k^*(x), \quad \text{with} \quad \nabla u_k^*(x) \in \overline{\Omega}_k, \quad \forall x \in \text{Dom}(\nabla u^*).$$

The setting in which  $\nu_2$  is supported on a union of disjoint sets is particularly relevant in Bayesian contexts where the posterior distribution may exhibit multimodality with well-separated local modes

(e.g., label switching in Bayesian mixture models, Jasra et al., 2005). In other cases, although the support of the posterior may not be strictly separable, it can often be well-approximated by a distribution with strongly separable support, where each component potential  $u_k^*$  can be interpreted as the local potential function corresponding to a particular local mode or region. In such a scenario, for each draw  $X$  from the reference distribution  $\mu$ , the optimal map effectively selects a local region via the index  $k(X) = \arg \max_{k \in I} u_k^*(X)$ , and then maps  $X$  to  $T^*(X) = \nabla u_{k(X)}^*(X)$  using the corresponding local potential  $u_{k(X)}^*$  (c.f. Lemma 5). Even when the target posterior  $\pi_n$  is not multimodal, one may still choose to represent the global potential  $u^*$  as the maximum over several convex functions, as motivated by Lemma 3, to enhance modeling flexibility and approximation capacity. This leads to the construction of the transport map class  $\mathcal{T}$  used in Section 3.1.

### 3 Optimal Transport for Bayesian Sampling

In this section, we formally introduce and address the following problem of learning an optimal generative model for efficient Bayesian sampling,

For a given reference distribution  $\mu$  on parameter space  $\Theta$ , how to approximate the optimal generative model  $(\mu, T^*)$  for sampling from the posterior  $\pi_n$ ? Here the optimality refers to  $T^*$  as the solution of the OT problem (MP) with  $\nu_1 = \mu$  and  $\nu_2 = \pi_n$ .

A key distinction between our approach and existing transport-based methods is that we approximate only the optimal transport map  $T^*$ , rather than any map  $T \in \mathcal{T}$  satisfying  $T_{\#}\mu = \pi_n$ . By imposing this additional constraint, we eliminate the non-uniqueness inherent in general transport maps, resulting in a solution that is stable, efficient, and interpretable. Furthermore, as discussed in Remark 2, any other transport map can be derived from  $T^*$ , thereby preserving full flexibility.

Recall that in our Bayesian setting, the posterior  $\pi_n$  is only known up to a normalization constant. Consequently, directly solving (MP) with  $\nu_1 = \mu$  and  $\nu_2 = \pi_n$  is computationally infeasible, and we must resort to alternative methods for approximating  $T^*$ . A common approach in the literature for addressing underdetermined systems — such as our constraint  $T_{\#}\mu = \pi_n$  — is to impose additional identifiability conditions via regularization. In our case, building on the KL-based formulation in (4)

for matching  $T_{\#}\mu$  to  $\pi_n$ , it is natural to consider the following regularized KL optimization:

$$\min_{T \in \mathcal{T}} \left\{ d_{\text{KL}}(T_{\#}\mu \parallel \pi_n) + \lambda \mathbb{E}_{\mu} [\|T(X) - X\|^2] \right\}, \quad (7)$$

where  $\lambda > 0$  is the regularization parameter and  $\mathcal{T}$  is a pre-specified class of transport maps. However, this approach introduces a bias term proportional to  $\lambda$ , and the computationally simplified equivalent formulation provided by Lemma 1 is not directly applicable unless additional constraints are imposed to ensure that each  $T$  along the optimization trajectory is invertible, which further complicates the implementation. Moreover, optimally tuning  $\lambda$  to balance the goodness-of-fit term and the regularization term can be computationally expensive.

Instead of relying on regularization, we propose a more direct constrained optimization approach for computing the optimal generative model by leveraging structural properties of the optimal transport map  $T^*$  — particularly those described in Lemma 2 when  $\theta$  is continuous. Furthermore, we generalize the characterization of the optimal transport map  $T^*$  to mixed settings where  $\theta$  may include discrete components, as commonly encountered in Bayesian latent variable models. In such cases, although the first property of Lemma 2 still applies and we can still model the transport map class  $\mathcal{T}$  as the space of all convex function gradients, Lemma 5 is no longer applicable to make Bayesian transport map learning computationally tractable, since the OT map  $T^*$  is no longer invertible (see Section 3.2 for further details).

The remainder of this section is organized as follows. Section 3.1 focuses on the continuous parameter setting, where Lemma 2 is applicable. In Section 3.2, we extend Lemma 2 to the mixed discrete-continuous setting by providing a finer characterization of the optimal transport map (c.f. Theorem 1), and we refine Lemma 1 for this case by deriving a more refined and computationally amenable optimization formulation (c.f. Lemma 6).

### 3.1 Optimal transport map with continuous parameters

We choose a reference distribution  $\mu$  that is absolutely continuous with respect to the Lebesgue measure on  $\mathbb{R}^p$ , such as the standard Gaussian  $\mathcal{N}(0, I_p)$ . Under this choice, Lemma 2 guarantees that the optimal transport map  $T^*$  is unique and can be characterized as the gradient of a convex

function  $u^*$ . More importantly, the *converse also holds*: if there exists a convex function  $u^*$  such that  $T^* = \nabla u^*$  pushes  $\mu$  forward to  $\pi_n$ , then  $T^*$  is the unique optimal transport map.

When  $\theta$  is continuous in  $\mathbb{R}^p$ , the posterior distribution  $\pi_n$  naturally has continuous probability density function. Therefore, according to the second and third properties of Lemma 2, the optimal transport map  $T^*$  is also differentiable and invertible. This implies that the convex potential function  $u^*$  defining  $T^* = \nabla u^*$  to be at least twice differentiable. Therefore, we can use the standard characterization of the twice differentiable convex function  $u$  as its Hessian  $\nabla^2 u = J_T$  being a positive semidefinite (p.s.d.) matrix on its domain. In addition, the Monge-Ampère equation in Lemma 2 imply  $J_T$  to be non-singular on the support  $\text{spt}(\mu)$  of  $\mu$ , meaning that  $\nabla^2 u$  should be positive definite (p.d.) (i.e.  $u$  strongly convex) and  $T$  should be globally invertible. These properties motivate us to specify the transport map class in (5) as

$$\mathcal{T} = \left\{ \nabla u \mid u : \text{spt}(\mu) \rightarrow \Theta, u \in C^2(\text{spt}(\mu)), \nabla^2 u \in \mathbb{R}^{p \times p} \text{ is p.d.} \right\}, \quad (8)$$

ensuring  $T^*$  to be the unique solution within  $\mathcal{T}$  such that  $T_{\#}\mu = \pi_n$ .

Since the transport class  $\mathcal{T}^*$  defined in (8) satisfies the assumptions of Lemma 1, the map  $T^*$  is the unique solution to the computationally feasible formulation (5) with this class, according to Lemma 2. In practice, we may employ a Monte Carlo approximation and choose an approximating class  $\mathfrak{T}$  as any parametric family that approximates the space  $\mathcal{T}$  of all twice differentiable and strongly convex functions over  $\text{spt}(\mu)$ , leading to the practical formulation:

$$\hat{T} = \arg \min_{T \in \mathfrak{T}} \frac{1}{M} \sum_{m=1}^M \left[ \log \tilde{\pi}_n(T(X_m)) + \log \det(J_T(X_m)) \right], \quad (9)$$

where  $\{X_m\}_{m=1}^M$  are i.i.d. samples from  $\mu$ , and  $\tilde{\pi}_n \propto \pi_n$  denotes any posterior density known up to a normalization constant.

**Construction of approximating class  $\mathfrak{T}$ .** In formulation (9), the approximation error between  $\hat{T}$  and  $T^*$  depends on the expressiveness of the chosen function class  $\mathfrak{T}$ . A widely used nonparametric class for approximating convex functions is the input convex neural network (ICNN) introduced by Amos et al. (2017). Due to their deep and flexible structure, ICNNs can be more effective for complex

problems and are universal approximators for convex functions (Geuken et al., 2025). However, our goal is to approximate the transport map as the gradient of a convex potential, and closeness in function values does not necessarily imply closeness in their gradients. In particular, the use of the popular rectified linear units (ReLU) activation functions in ICNNs leads to non-differentiable potentials, which is undesirable in our setting. Therefore, in our implementation, we adopt a simpler approximating family, partly motivated by structural properties of the optimal transport map (e.g., Lemma 3). We find that this choice yields competitive performance in both simulation studies and real-world applications.

To begin constructing the approximating class  $\mathfrak{T}$ , we first introduce a class of convex building blocks, referred to as convex units, motivated by the following lemma.

**Lemma 4.** *For constants  $\alpha, \beta \in \mathbb{R}^p$  and  $w, v \in \mathbb{R}$ , and an increasing and bounded univariate function  $\varphi$  defined on  $\mathbb{R}$ , the following function defined by*

$$f(x; \alpha, \beta, w, v) = \int_{-\infty}^{\langle \alpha, x \rangle + w} \varphi(u) \, du + \langle \beta, x \rangle + v \quad (10)$$

is a convex function of  $x \in \mathbb{R}^p$ .

The proof is provided in Section C.3. In our implementation, we adopt the following choices for  $\varphi$ : 1. the Tanh function:  $\varphi(x) = \frac{e^x - e^{-x}}{e^x + e^{-x}}$ ; 2. the Softsign function:  $\varphi(x) = \frac{x}{1+|x|}$ ; 3. the Square Nonlinearity (SQNL) function:  $\varphi(x) = \text{sign}(x)1_{|x|>2} + (x - \text{sign}(x)\frac{x^2}{4})1_{|x|\leq 2}$ . It is straightforward to verify that these functions satisfy the constraints in Lemma 4 while introducing nonlinearity to enhance flexibility. In particular, the parameter  $\alpha > 0$  in the convex unit controls the degree of nonlinearity: over any compact set  $\mathcal{C} \subset \mathbb{R}^p$ , a smaller  $\alpha$  makes the convex unit closely resemble an affine transformation for  $x \in \mathcal{C}$ . Adding an affine term  $\langle \beta, x \rangle + w$  preserves the convexity of the function  $g(x)$ , while further increasing its expressiveness.

With the convex unit, we can now define our family  $\mathcal{U}_{L,M}$  of convex functions  $u$  to approximate the optimal convex potential  $u^*$  as

$$\mathcal{U}_{L,M} = \left\{ u : \mathbb{R}^p \rightarrow \mathbb{R} \left| u(x) = \max_{k \in [L]} u_k(x), u_k(x) = \sum_{m=1}^M f(x; \alpha_m^{(k)}, \beta_m^{(k)}, w_m^{(k)}, v_m^{(k)}), \right. \right. \quad (11)$$

$$\left. \left. \alpha_m^{(k)} \in \mathbb{R}^p, \beta_m^{(k)} \in \mathbb{R}^p, w_m^{(k)} \in \mathbb{R}, v_m^{(k)} \in \mathbb{R}, \text{ for all } k \in [L] \text{ and } m \in [M] \right\},$$

where  $L$  is the number of local potential functions  $u_k$  in the maximum, and  $M$  is the number of convex units used to define each  $u_k$ . The corresponding transport map class  $\mathfrak{T}$  used in (9) is then defined as  $\mathfrak{T} = \{T : \mathbb{R}^p \rightarrow \mathbb{R}^p \mid T = \nabla u(x), u \in \mathcal{U}_{L,M}\}$ .

A few observations are worth noting. First, since the sum and maximum of finitely many convex functions are themselves convex, all functions in  $\mathcal{U}_{L,M}$  are valid convex functions. Second, any convex function  $u$  over  $\mathbb{R}^p$  can be well approximated by a function in  $\mathcal{U}_{L,M}$  for sufficiently large  $L$  and  $M$ , since the union  $\bigcup_{L \geq 1, M \geq 1} \mathcal{U}_{L,M}$  contains all max-affine functions, which are known to approximate any convex function arbitrarily well (Magnani and Boyd, 2009). Third, the use of the maximum operator in constructing functions in  $\mathcal{U}_{L,M}$  is also inspired by Lemma 3, which shows that when the target distribution contains multiple well-separated clusters, the corresponding optimal potential function  $u^*$  naturally takes the form of a maximum over several local potential functions, each associated with a specific cluster. Without incorporating the max operation, the number of convex units required to approximate  $u^*$  may grow exponentially with the number of clusters. Last but not least, the following lemma provides a computational strategy for evaluating the transport map  $T = \nabla u = \nabla \max_{k \in [L]} u_k$ , as well as its Jacobian — both of which are needed to implement the gradient descent algorithm for solving problem (9). This facilitates computing the gradient of the maximum of  $L$  convex functions efficiently.

**Lemma 5.** *Let  $\{u_k\}_{k=1}^L$  be  $L$  twice differentiable and convex functions over  $\mathbb{R}^p$ , and  $\iota(x) := \arg \max_{k \in [L]} u_k(x)$  for each  $x \in \mathbb{R}^p$ . Then the gradient  $T(x) = \nabla \max_{k \in [L]} u_k(x)$  is  $\nabla u_{\iota(\theta)}(x)$ , and the Jacobian matrix of  $T$  at  $x$  is  $J_T(x) = \nabla^2 u_{\iota(x)}(x)$ .*

This lemma states that to compute the gradient of the maximum over a set of convex functions, one first identifies the convex function with the largest evaluation — determined partly by the intercept  $v$  in the convex unit, which also governs the separation of local regions associated with each local potential function  $u_k$  — and then takes the gradient of the selected convex function. Ideally, the number of convex functions  $L$  would match the number of distinct regions or modes of the target distribution  $\pi_n$ . When the number of modes is unknown, we can begin with a small value of  $L$  and increase it as needed. For practical implementation, the max operation is replaced with a Softmax transformation to ensure gradient tractability and avoid vanishing gradients.

### 3.2 Optimal transport map with mixed parameters

In a more general setting where  $\theta$  consists of both continuous and discrete components, referred to as mixed parameters or variables, we decompose  $\theta = (\tau, \zeta)$ , where  $\tau \in [K] := \{1, 2, \dots, K\}$  denotes the discrete component with  $K$  levels, and  $\zeta \in \mathbb{R}^p$  represents the continuous component of dimension  $p$ .

Since  $\tau$  is discrete, we introduce  $K$  vector embedding  $\{b_k\}_{k=1}^K$  in  $\mathbb{R}^r$  to encode categorical information. The choice of embeddings depends on the nature of  $\tau$ . For example, if  $\tau$  is a nominal variable, then order does not matter and we choose  $\{b_k\}_{k=1}^K$  as the  $K$  vertices of a regular polyhedron in  $\mathbb{R}^{K-1}$  ( $r = K - 1$ ), ensuring uniform pairwise distance  $\|b_k - b_l\|_2 = 1$  for  $k \neq l$ . If  $\tau$  is ordinal, we choose  $\{b_k\}_{k=1}^K$  as an increasing sequence in  $\mathbb{R}$  ( $r = 1$ ), where  $b_{k+1} - b_k$  quantifies the gap between levels  $k$  and  $k + 1$ .

Let us also decompose the input variable  $x$  realized by the reference distribution into  $x = (x^{(1)}, x^{(2)}) \in \mathbb{R}^r \times \mathbb{R}^p$  and write the transport map  $T$  as  $T = (T^{(1)}, T^{(2)})$ , where  $T^{(1)} : \mathbb{R}^r \times \mathbb{R}^p \rightarrow [K]$  transforms to the discrete component and  $T^{(2)} : \mathbb{R}^r \times \mathbb{R}^p \rightarrow \mathbb{R}^p$  transforms to the continuous component. Since we continue to use the standard Gaussian  $\mathcal{N}(0, I_{r+p})$  as the reference distribution  $\mu$ , Lemma 2 guarantees that the optimal transport (OT) problem is equivalent to the Monge problem with mixed variables, formulated as follows:

$$\begin{aligned}
 \text{(MPm)} \quad & \inf_{T=(T^{(1)}, T^{(2)})} \int_{\mathbb{R}^r \times \mathbb{R}^p} \left[ \underbrace{\kappa \|x^{(1)} - b_{T^{(1)}(x)}\|_2^2}_{\text{discrete part cost}} + \underbrace{\|x^{(2)} - T^{(2)}(x)\|_2^2}_{\text{continuous part cost}} \right] d\mu(x), \\
 \text{s.t.} \quad & T_{\#}\mu = \pi_n \quad \text{and} \quad T^{(1)}(x) \in [K], \quad \text{for all } x = (x^{(1)}, x^{(2)}) \in \mathbb{R}^r \times \mathbb{R}^p,
 \end{aligned}$$

where  $\kappa > 0$  is a weighting parameter controlling the relative impact of the discrete component cost in the overall cost. By default, we choose  $\kappa = 1$  throughout the paper.

In this case, since the posterior  $\pi_n$  contains singularity due to the discrete component, the second and third properties of Lemma 2 concerning absolutely continuous  $\nu_2$  are no longer applicable. In particular, for each fixed  $x^{(2)} \in \mathbb{R}^p$ , the convex function  $u(\cdot, x^{(2)})$  in the lemma becomes a piecewise-linear function over  $\mathbb{R}^r$  (c.f. Theorem 1 below), making the optimal transport map  $T = \nabla u$  non-invertible. Consequently, Lemma 1 does not apply, and we need to find another

finer characterization of  $T^*$  and the associated convex function  $u^*$ , while keeping the computation tractable and efficient. The following lemma provides such a characterization, suggesting that we should treat the continuous and discrete components separately when modeling  $T$  or  $u$ .

**Theorem 1.** *Suppose the reference distribution  $\mu$  is absolutely continuous over  $\mathbb{R}^r \times \mathbb{R}^p$  and the target distribution  $\pi_n$  is defined over  $\theta = (\tau, \zeta)$ , where  $\tau \in [K]$  and  $\zeta \in \mathbb{R}^p$ . Then the optimal potential function  $u^*$  associated with  $T^* = (T^{*(1)}, T^{*(2)})$  in problem (MPm) takes the form*

$$u^*(x^{(1)}, x^{(2)}) = \kappa \max_{k \in [K]} \{ \langle x^{(1)}, b_k \rangle + \phi_k(x^{(2)}) \},$$

where  $b_k \in \mathbb{R}^r$  is the pre-specified embedding vector for category  $k$ , and  $\phi_k : \mathbb{R}^p \rightarrow \mathbb{R}$  is a convex function. The corresponding OT map  $T^* = (T^{*(1)}, T^{*(2)})$  is

$$\begin{cases} \tau = T^{*(1)}(x^{(1)}, x^{(2)}) = \arg \max_{k \in [K]} \{ \langle x^{(1)}, b_k \rangle + \phi_k(x^{(2)}) \}, \\ \zeta = T^{*(2)}(x^{(1)}, x^{(2)}) = \kappa \nabla \phi_\tau(x^{(2)}). \end{cases} \quad (12)$$

Furthermore, if for any category  $k \in [K]$ , the conditional posterior distribution  $\pi_n(\zeta \mid \tau = k)$  is absolutely continuous with respect to the Lebesgue measure on  $\mathbb{R}^p$ , then the function  $\phi_k$  is at least twice differentiable and strongly convex, ensuring that  $\nabla \phi_k$  is both differentiable and invertible.

According to this result, the function  $u^*$  is piecewise linear in  $\mathbb{R}^r$  due to the linear term  $\langle x^{(1)}, b_k \rangle$ . This causes probability mass accumulation in discrete component  $\tau$  and makes  $T^*$  non-invertible. When  $\mu$  is a product measure over  $\mathbb{R}^r \times \mathbb{R}^p$ , the  $k$ -th map  $T_k^* := \nabla \phi_k$  in Theorem 1 can be interpreted as the optimal transport map that pushforwards the marginal of  $\mu$  over  $\mathbb{R}^p$  to the conditional posterior  $\pi_n(\zeta \mid \tau = k)$ . Thus, the overall optimal transport map  $T^*$  can be viewed as a location-dependent ‘‘mixture’’ of the local maps  $\{T_k^*\}_{k=1}^K$ . Duan (2021) also proposed a random transport map constructed as a mixture of transport maps  $\{T_i\}_{i=1}^N$ , motivated by Bayesian nonparametric approximations of conditional densities (Dunson et al., 2007). In their method, each point is transported by map  $T_i$  with a location-dependent probability  $\omega_i$ , drawn from  $\{\omega_i\}_{i=1}^N$ . However, since they consider only location-scale transformations for the  $T_i$ ’s, their approach is costly for representing complex target distributions and scales poorly when handling discrete variables. El Moselhy and Marzouk (2012) proposed an alternative approach using lower-triangular transport maps. However, these maps are

not uniquely defined, and additional constraints must be imposed to ensure identifiability, which complicates the optimization. Furthermore, their reliance on polynomial parameterizations leads to exponential growth in computational complexity as the dimensionality increases.

In the further special case where  $\mu$  is the standard Gaussian distribution  $\mathcal{N}(0, I_{r+p})$ , the first equation in (12) resembles a multi-class extension of the Probit model. Given  $x^{(2)}$ , the latent score for class  $k$  is given by  $\langle x^{(1)}, b_k \rangle + \phi_k(x^{(2)})$ , and follows the distribution  $\langle x^{(1)}, b_k \rangle + \phi_k(x^{(2)}) \mid x^{(2)} \sim N(\phi_k(x^{(2)}), \|b_k\|^2)$ , with the final label assigned to the class with the highest latent score. Meanwhile, the continuous component  $\zeta$  is generated from the conditional posterior  $\pi_n(\zeta \mid \tau)$  by pushing forward the marginal reference distribution  $\mathcal{N}(0, I_p)$  through the transport map  $T_\tau^*$ . This structured factorization of the transport map naturally leads to the following lemma, which serves as a counterpart to Lemma 1 and forms a key building block for efficient computation in the mixed-variable setting.

**Lemma 6** (Optimization objective for mixed parameters). *Let  $T : \mathcal{X} \rightarrow \mathcal{Y}$  be a transport map that pushforwards  $\mu$  to  $\pi_n$ , where  $\mathcal{X} = \mathcal{X}_1 \times \mathcal{X}_2 := \mathbb{R}^r \times \mathbb{R}^p$  and  $\mathcal{Y} = \mathcal{Y}_1 \times \mathcal{Y}_2 := [K] \times \mathbb{R}^p$ . We define the intermediate transport map  $\tilde{T} : \mathcal{Y}_1 \times \mathcal{X}_2 \rightarrow \mathcal{Y}_1 \times \mathcal{Y}_2$  induced by  $T$  as*

$$\begin{pmatrix} \tau \\ x^{(2)} \end{pmatrix} \mapsto \begin{pmatrix} \tau \\ \zeta = \kappa \nabla \phi_\tau(x^{(2)}) \end{pmatrix}.$$

Then, the optimization problem in (4), with  $\mathcal{T}$  chosen as the class of transport maps taking the form of (12) in Theorem 1, is equivalent to:

$$\min_{T \in \mathcal{T}} \mathbb{E}_{(X^{(1)}, X^{(2)}) \sim \mu} \left[ \log \mathbb{P}(\tau \mid X^{(2)}) - \log \pi_n \circ \tilde{T}(\tau, X^{(2)}) - \log |\det(J_{\tilde{T}}(\tau, X^{(2)}))| \right], \quad (13)$$

with  $\tau = \arg \max_{k \in [K]} \{ \langle X^{(1)}, b_k \rangle + \phi_k(X^{(2)}) \}$ .

The proof of this lemma is provided in Section C.5.

To evaluate the objective function in the optimization problem (13) for a given transport map  $T$ , we apply the Monte Carlo method by approximating the expectation with an empirical average. Specifically, we first generate  $N$  i.i.d. samples  $\{x_1, x_2, \dots, x_N\}$  from  $\mu$ , and then compute the corresponding transformed variables  $\{\theta_1, \theta_2, \dots, \theta_N\}$  via the transport map  $T$  defined in (28), where

each  $\theta_i = (\tau_i, \zeta_i)$  with  $\zeta_i = \nabla \phi_{\tau_i}(x_i^{(2)})$  and

$$\tau_i = \arg \max_{k \in [K]} \left\{ \langle x_i^{(1)}, b_k \rangle + \phi_k(x_i^{(2)}) \right\}, \quad \text{for } i = 1, 2, \dots, N.$$

The conditional probabilities  $\mathbb{P}(\tau | X^{(2)})$  can also be estimated using the Monte Carlo method; additional computational details are provided in Section A.2.

## 4 Applications in Bayesian Inference

In the previous section, we introduced a general framework for constructing transport maps that enable sampling from distributions with intractable normalizing constants. In this section, we further elaborate on several applications of our method to Bayesian inference.

Concretely, we begin with two applications that leverage specific designs of the approximating class  $\mathfrak{T}$  for the transport class  $\mathcal{T}$  to enhance computational efficiency. In the first application, we demonstrate that when the posterior is approximately Gaussian — as guaranteed by the celebrated Bernstein–von Mises theorem for regular parametric models with large sample sizes — an affine transport class  $\mathfrak{T}_{\text{aff}}$  is sufficient to preserve approximation quality up to the statistical accuracy of the problem, while significantly reducing computational complexity and enabling fast, accurate posterior approximation. In the second application, we incorporate the mean-field approximation technique from variational inference (Blei et al., 2017; Zhang and Yang, 2024) to improve scalability in Bayesian latent variable models. This approach leads to a mean-field transport map class  $\mathfrak{T}_{\text{MF}}$ , which substantially reduces the effective cardinality of the discrete variable  $\tau$  and enhances computational scalability. Finally, we present a third application for statistical inference that is uniquely enabled by our optimal transport map–based sampling framework: it enables novel posterior summaries and uncertainty quantification via the computation of OT-derived multivariate ranks, along with the construction of center-outward quantile contours and sign curves as proposed by Hallin et al. (2021). These tools provide powerful new capabilities for Bayesian exploratory analysis and visualization.

## 4.1 Approximately Gaussian posteriors

The celebrated Bernstein–von Mises (BvM) theorem for parametric models (Le Cam and Yang, 2000; van der Vaart, 2000) states that under the frequentist perspective where the data  $\{Z_1, \dots, Z_n\}$  are i.i.d. samples from the true data generating model  $p(\cdot | \theta_0)$  with  $\theta_0$  denoting the true parameter, the posterior distribution  $\pi_n(\theta) = p(\theta | Z^n)$  is asymptotically normal, with its mean close to the maximum likelihood estimator (MLE) and its variance approximated by the inverse of the total Fisher information matrix. This classical result enables a significant improvement in computational efficiency by allowing us to simplify the approximating family of transport maps while maintaining high approximation accuracy. In particular, the following theorem implies that a linear transport map is sufficient to approximate a posterior distribution that approaches a Gaussian, while still preserving the statistical accuracy required for inference.

**Lemma 7** (Linear transport maps for nearly Gaussian posteriors). *Suppose the posterior  $\pi_n$  satisfies the following Gaussian approximation bound:*

$$d_{\text{KL}}\left(\pi_n \left\| \mathcal{N}\left(\hat{\theta}_n, \frac{1}{n}I_{\theta_0}^{-1}\right)\right.\right) = \mathcal{O}_p(n^{-1/2}), \quad \text{as } n \rightarrow \infty, \quad (14)$$

where  $\hat{\theta}_n$  denotes the MLE, and  $I_{\theta_0}$  is the nonsingular Fisher information matrix at the true parameter  $\theta_0$ . Then, with the choice of affine transport map class  $\mathfrak{T}_{\text{aff}}$  of:

$$\mathfrak{T}_{\text{aff}} = \left\{ T : \mathbb{R}^p \rightarrow \Theta \mid T(x) = m + \frac{1}{\sqrt{n}}S^T x, \quad x \in \mathbb{R}^p, \quad \text{with } m \in \mathbb{R}^p \text{ and } S \in \mathbb{R}^{p \times p} \text{ being p.d.} \right\}, \quad (15)$$

then the estimated transport map  $\hat{T}$ , as defined in equation (9), satisfies

$$d_{\text{KL}}(\hat{T}_{\#}\mu \parallel \pi_n) = \mathcal{O}_p(n^{-1/2}), \quad \text{as } n \rightarrow \infty.$$

The proof relies on the fact that a sample from the asymptotic Gaussian approximation  $\mathcal{N}(\hat{\theta}_n, n^{-1}I_{\theta_0}^{-1})$  can be expressed as an affine transformation of the form  $\tilde{T}(X) = \hat{\theta}_n + n^{-1/2}I_{\theta_0}^{-1/2}X$  belonging to  $\mathfrak{T}_{\text{aff}}$ , where  $X \sim \mu = \mathcal{N}(0, I_p)$  and  $I_{\theta_0}^{-1/2}$  denotes the matrix square root of  $I_{\theta_0}^{-1}$ . Since  $\hat{T}$  minimizes the KL divergence objective, the resulting risk value  $d_{\text{KL}}(\hat{T}_{\#}\mu \parallel \pi_n)$  cannot exceed that in (14), and

the result follows.

The Gaussian approximation assumption in (14) generally holds for parametric models with a fixed number of parameters under a standard set of regularity conditions; see, for example, Katsevich (2023); Zhang and Yang (2024). Under the same set of regularity conditions, the MLE satisfies the asymptotic normality, that is,  $\sqrt{n}(\hat{\theta}_n - \theta_0) \xrightarrow{d} \mathcal{N}(0, I_{\theta_0}^{-1})$  as  $n \rightarrow \infty$ . As a consequence, credible intervals constructed using the approximation  $\hat{T}_{\#}\mu$  to the posterior  $\pi_n$  can attain their nominal coverage levels asymptotically as  $n \rightarrow \infty$ . Therefore, this numerical approximation with  $\mathfrak{T}_{\text{aff}}$  does not compromise statistical accuracy.

For implementation, we parameterize the positive definite matrix  $S$  in the class  $\mathfrak{T}_{\text{aff}}$  via its Cholesky root  $L$ , a lower triangular matrix with positive diagonal entries such that  $S = LL'$ . Under this parameterization, the log-determinant term associated with the affine transformation  $T(x) = m + \frac{1}{\sqrt{n}}S^T x$  simplifies to  $\log |\det(J_T)| = 2 \sum_{i=1}^p \log L_{ii} - \frac{1}{2}p \log n$ . This formulation reduces computational cost of the implementation and improves numerical stability.

## 4.2 Bayesian latent variable models

Many Bayesian latent variable models involve multiple latent variables  $\{c_j\}_{j=1}^J$ , where the cardinality of the discrete latent space often grows exponentially with the number  $J$  of latent variables. This imposes serious computational challenges for sampling. For example, in Gaussian mixture models and hidden Markov models (Rabiner, 1989), the latent variables  $c_j$  are observation-specific, so  $J$  equals to the sample size  $n$ . In spike-and-slab regression models (Ishwaran and Rao, 2005), each  $c_j$  is a binary indicator denoting the inclusion of the  $j$ -th covariate, and  $J$  equals the total number of covariates.

In this subsection, we focus on the Bayesian Gaussian Mixture Model (GMM) as a representative example of Bayesian latent variable models, and illustrate how to construct and approximate the optimal transport map for the posterior distribution over the mixed parameter  $\theta$ , which includes both model parameters and a large number of discrete latent variables. To improve scalability, we apply Theorem 1, which characterizes the optimal transport map  $T^*$ , and incorporate the mean-field approximation technique from variational inference (Blei et al., 2017; Zhang and Yang, 2024) to construct a transport map class  $\mathfrak{T}$  for approximating  $T^*$ .

Specifically, we consider the standard hierarchical formulation of GMM with  $K$  isotropic Gaussian components in  $d$ -dimensions, where  $n$  observations  $Z^{(n)} = (Z_1, Z_2, \dots, Z_n)^T$  and their observation-specific latent variables  $\{c_1, c_2, \dots, c_n\}$  follow

$$\begin{aligned} Z_i | c_i, \{m_k\}_{k=1}^K &\sim \mathcal{N}(m_{c_i}, \sigma^2 I_d), & i = 1, \dots, N, \\ c_i &\sim \text{Categorical}\left(\frac{1}{K}, \dots, \frac{1}{K}\right), & i = 1, \dots, N, \\ m_k &\sim \mathcal{N}(m_0, \lambda^2 I_d), & k = 1, \dots, K. \end{aligned}$$

Here,  $m_k$  represents the mean of clusters  $k$ , and  $c_i$  is the latent variables indicating the cluster assignment of  $Z_i$ . The first two lines together specify the complete data likelihood and the third line specifies the prior of model parameter  $\zeta = (m_1, m_2, \dots, m_K)^T$ . Based on this hierarchical formulation and the Bayes formula, we can express the joint posterior distribution  $\pi_n$  of  $\theta = (\tau, \zeta) : = (\{c_i\}_{i=1}^n, \{m_k\}_{k=1}^K)$  as

$$\pi_n(\theta) = \pi(\tau, \zeta | Z^{(n)}) \propto \prod_{i=1}^n [p(Z_i | c_i, \zeta) \cdot p(c_i)] \cdot \prod_{k=1}^K \pi(m_k).$$

To construct the transport map in (12), we first specify the embedding for the  $n$  latent variables  $\{c_i\}_{i=1}^n$ . Since the  $n$  latent variables  $\{c_i\}_{i=1}^n$  take the same set of unordered labels  $[K]$ , we adopt the strategy in Section 3.2 by assign a vector  $b_k \in \mathbb{R}^{K-1}$  to each label  $k \in [K]$  such that  $\|b_k - b_\ell\| = 1$  for each distinct pair  $(k, \ell) \in [K]^2$ . The overall embedding  $\tau = (c_1, \dots, c_n)$  is then  $b_\tau = (b_{c_1}, b_{c_2}, \dots, b_{c_n}) \in \mathbb{R}^{(K-1)n}$ . With this choice, the reference distribution  $\mu$  is defined over  $\mathcal{X} = \mathcal{X}_1 \times \mathcal{X}_2 = \mathbb{R}^r \times \mathbb{R}^p$ , where  $r = (K-1)n$  and  $p = Kd$ . We adopt the standard choice of  $\mu$  as the standard Gaussian distribution  $\mathcal{N}(0, I((K-1)n + Kd))$ . Note that in this model, the cardinality of the discrete variable  $\tau$  is  $K^n$ , which grows exponentially with  $n$ , implying that  $K^n$  convex functions — denoted  $\phi_{c_1, c_2, \dots, c_n}$  for each combination  $(c_1, c_2, \dots, c_n) \in [K]^n$  — would need to be estimated, according to Theorem 1. Therefore, computing the optimal transport map  $T^*$  in (12) becomes quickly infeasible as  $n$  increases.

To address this computational challenge, we propose a “mean-field” approximation to reduce the complexity of the transport map. Instead of estimating an exponentially large number of functions, we decompose the collection of convex functions  $\{\phi_{c_1, c_2, \dots, c_n} : c_i \in [K], i \in [n]\}$  as a sum of  $n$

individual convex functions:

$$\phi_{c_1, c_2, \dots, c_n}(x^{(2)}) = \sum_{i=1}^n \phi_{c_i}^{(i)}(x^{(2)}), \quad (16)$$

which reduces the number of convex functions from  $K^n$  to  $Kn$ . The resulting transport map from (12) can be correspondingly factorized as  $T^* = (T_1^{*(1)}, T_2^{*(1)}, \dots, T_n^{*(1)}, T^{*(2)})$ , where

$$\begin{cases} c_i = T_i^{*(1)}(x_i^{(1)}, x^{(2)}) = \arg \max_{k \in [K]} \left\{ \langle x_i^{(1)}, b_k \rangle + \phi_k^{(i)}(x^{(2)}) \right\}, & \text{for } i \in [n], \\ \zeta = T^{*(2)}(\{x_i^{(1)}\}_{i=1}^n, x^{(2)}) = \kappa \sum_{i=1}^n \nabla \phi_{c_i}^{(i)}(x^{(2)}), \end{cases} \quad (17)$$

for  $x_i^{(1)} \in \mathbb{R}^{K-1}$  and  $x^{(2)} \in \mathbb{R}^p$ . We refer to the collection  $\mathfrak{T}_{\text{MF}}$  of all transport maps of this form as the mean-field transport map class. Then, our transport map estimator  $\widehat{T}$  is obtained by optimizing the objective in (13) over all  $T \in \mathfrak{T}_{\text{MF}}$ .

The approximation in (17) follows the spirit of mean-field variational inference (Blei et al., 2017) by simplifying the dependency structure among latent variables. Interestingly, our approach lies between a fully flexible model and the conventional mean-field approximation, which assumes a fully factorized approximating family. Specifically, the scheme in (16) can be interpreted as imposing a partial conditional independence structure among the latent variables  $\{c_i\}_{i=1}^n$ , given the model parameter  $\zeta$  (determined by  $x^{(2)}$ ), thereby significantly relaxing the full independence assumption of the standard mean-field approximation. Given that Yang et al. (2020) have shown consistency for the conventional mean-field approximation in estimating parameters of Bayesian latent variable models, we expect our more flexible scheme to exhibit similar consistency properties. Our numerical results in Section 5.3 further demonstrate that the simplified structure in (16) effectively captures the target posterior distribution.

To further improve the computational scalability of the convex functions  $\phi_k^{(i)}$  with respect to the sample size  $n$ , we may set the relative weight parameter  $\kappa$  in (MPm) to  $n^{-1}$ . With this choice, the second equation in (17) for generating  $\zeta$  reduces to an average, making the computation less

sensitive to large  $n$ ,

$$\zeta = T_B^{(2)}(\{x_i^{(1)}\}_{i=1}^n, x^{(2)}) = \frac{1}{n} \sum_{i=1}^n \nabla \phi_{c_i}^{(i)}(x^{(2)}),$$

where  $\nabla \phi_{c_i}^{(i)}(x^{(2)})$  can be interpreted as the message that observation  $Z_i$  conveys about the cluster centers. Another justification for choosing  $\kappa$  arises from the structure of the concatenated discrete variable  $\tau$ , which consists of  $n$  latent variables. In this case, the corresponding discrete component of the cost in (MPm) becomes

$$\kappa \sum_{i=1}^n \|x_i^{(1)} - T_{B,i}^{(1)}(x_i^{(1)}, x^{(2)})\|^2.$$

To prevent this discrete cost — which scales as  $\mathcal{O}(n\kappa)$  — from dominating the continuous part of the cost, which is  $\mathcal{O}(1)$ , it is appropriate to choose  $\kappa = \mathcal{O}(n^{-1})$ . To further simplify computation, we may approximate each additive component  $\phi_{k_i}^{(i)}(x^{(2)})$  in (16) using an additive structure of the form  $\sum_{k=1}^K \phi_{k_i,k}^{(i)}(x_k^{(2)})$ , where  $x_k^{(2)} \in \mathbb{R}^d$  denotes the  $k$ -th component of  $x^{(2)}$  associated with the  $k$ -th cluster mean vector  $m_k$ . This corresponds to a block mean-field approximation for the model parameter  $\zeta = (m_1, m_2, \dots, m_K)^T$  over the  $K$  (blocks of) parameters  $\{m_k\}_{k=1}^K$ , preserving within-block dependencies while ignoring between-block dependencies. Similarly, a fully factorized mean-field approximation for the model parameter  $\zeta$  can be obtained by further decomposing each convex function  $\phi_{k_i,k}^{(i)}(x_k^{(2)})$  with respect to the individual coordinates  $x_k^{(2)} = (x_{k,1}^{(2)}, x_{k,2}^{(2)}, \dots, x_{k,d}^{(2)})$  in  $\mathbb{R}^d$ . Further details are provided in Section A.3.

### 4.3 Posterior summaries via OT-derived center-outward ranks and quantiles

Constructing credible intervals or regions is essential for uncertainty quantification in Bayesian inference, as it supports informed decision-making and risk assessment in downstream tasks. However, defining meaningful quantiles for multivariate posteriors remains a complex and challenging problem. Various approaches have been proposed in the literature, including marginal quantiles for each

parameter, ellipsoidal quantiles for approximately Gaussian posteriors, copula-based quantiles, Tukey depth contours (Tukey, 1975) and data depth (Liu, 1990). More recently, Hallin et al. (2021) introduced OT-derived center-outward quantiles, where quantile contours of a reference distribution — such as a standard Gaussian — are mapped through an optimal transport map  $T^*$ . These quantiles inherit desirable properties from their univariate counterparts, making them a promising tool for multivariate exploratory analysis and visualization. In addition to the center-outward quantile contours, Hallin et al. (2021) also propose center-outward ranks  $R_{\pm}$ , which, however, requires evaluating the inverse map  $(T^*)^{-1}$ .

In this subsection, we show how our method facilitates the construction of center-outward ranks and quantiles for multivariate distributions, including a banana-shaped distribution and a multimodal mixture example. These results demonstrate that our approach preserves the geometric structure of the target distribution while providing meaningful directional information.

We begin with examples of quantile contours. For complex posterior distributions, where the normalizing constant is unknown and only samples from  $\pi_n$  are available, quantile estimation becomes particularly challenging. Common practices include estimating marginal quantiles from the samples or using kernel density estimation (KDE) methods to approximate quantile boundaries. While these approaches are straightforward, the number of samples from  $\pi_n$  required can grow exponentially with the parameter dimension  $p$ , and their efficiency is affected by both the sampling procedure and the approximation errors introduced by KDE.

Our approach is closely related to Hallin et al. (2021) in that we also aim to find the optimal transport map  $T^*$  from a reference distribution  $\mu$  to the target distribution, and both methods leverage the property that  $T^*$  is the gradient of a convex function. The key difference is that we learn this mapping using the unnormalized density function of  $\pi_n$ , whereas Hallin et al. (2021) estimate  $T^*$  from the empirical distribution of the data, such that the resulting quantiles are defined only on the observed data points. In our approach, we choose the reference distribution to be a standard Gaussian and construct center-outward quantile contours by mapping its quantile circles through the estimated OT map  $\hat{T}$ . The examples below illustrate the advantages of our method.

**Example 1** (Non-convex “banana” distribution). *To illustrate the effectiveness of our method in preserving non-convex quantile shapes, we consider the banana-shaped distribution from Hallin et al.*

(2021), defined as:

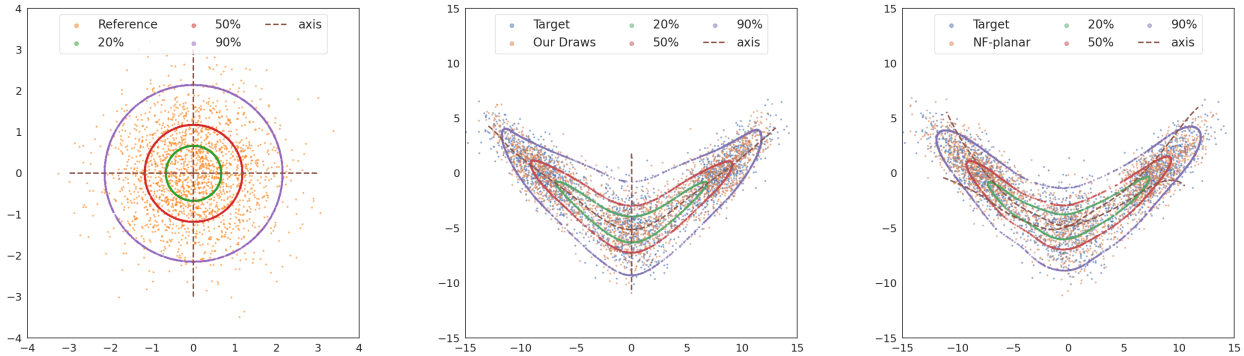
$$\frac{3}{8}\mathcal{N}(-8m_h, \Sigma_1) + \frac{3}{8}\mathcal{N}(8m_h, \Sigma_2) + \frac{1}{4}\mathcal{N}(-5m_\nu, \Sigma_3)$$

where  $m_h = (1, 0)^T$ ,  $m_\nu = (0, 1)^T$ ,  $\Sigma_1 = \begin{pmatrix} 5 & -4 \\ -4 & 5 \end{pmatrix}$ ,  $\Sigma_2 = \begin{pmatrix} 5 & 4 \\ 4 & 5 \end{pmatrix}$ ,  $\Sigma_3 = \begin{pmatrix} 4 & 0 \\ 0 & 1 \end{pmatrix}$ .

This distribution is particularly challenging due to its non-convex shape, and meaningful quantile contours must accurately preserve this structure. To generate center-outward quantiles, say, the  $q$ -quantile, we simply draw samples from the unit sphere  $\{x \in \mathbb{R}^2 : \|x\|_2^2 = -2 \ln(1 - q)\}$ , which corresponds to the quantiles of  $\mathcal{N}(0, I_2)$ , and map them through the estimated transport map  $\hat{T}$ . In Figure 1, we map the quantile contours (20%, 50%, and 90%) and the axes of the reference measure  $\mu$ , represented by sign curves from Hallin et al. (2021), to the banana-shaped distribution. We compare our method against another alternative transport map based on normalizing flows (NF) with planar transformers (Rezende and Mohamed, 2015). Note that transport Monte Carlo (Duan, 2021), which is included in our simulation study in Section 5, is not applicable in this context because it relies on a standard multivariate uniform reference distribution. This distribution is not *spherical uniform* (as defined in Chernozhukov et al., 2017) and therefore cannot be used to construct center-outward quantiles.

As shown in Figure 1, both methods produce samples that resemble the shape of the true distribution. However, our method, which employs a non-crossing map, preserves the non-convex shape of the quantile contours much more effectively. In addition, our method provides more accurate directional information: the probability mass between each pair of axes is expected to be equal, and only our approach successfully partitions the target distribution into four regions of equal probability. In contrast, although the NF-planar approach captures the general shape of the quantile regions, the distorted sign curves reveal a loss of directional information, which may lead to incorrect inferences about conditional dependencies among parameters.

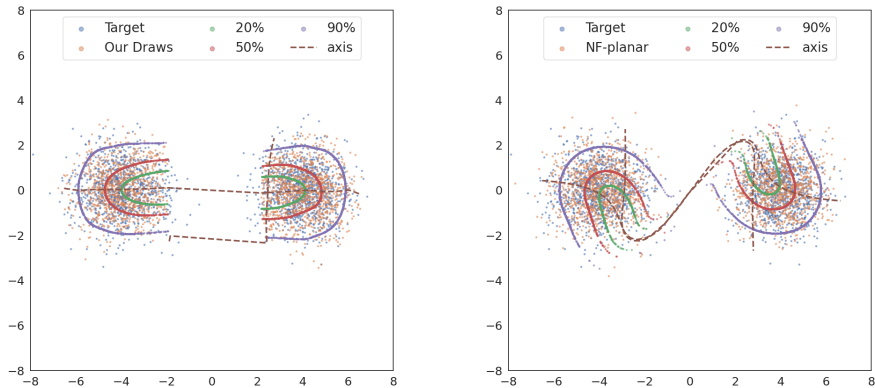
Next, we evaluate our method on a multimodal distribution, specifically the mixture of two bivariate Gaussian distributions considered in Hallin et al. (2021). The target distribution is given by  $\frac{1}{2}\mathcal{N}(-4m_h, I_2) + \frac{1}{2}\mathcal{N}(4m_h, I_2)$ . We set  $L = 2$  in our approximation class (11), allowing each mode to be captured by a separate convex function. Figure 2 shows the approximated posterior samples and the corresponding center-outward quantiles produced by our method and NF-planar.



(a) Reference distribution  $\mathcal{N}(0, I_2)$                       (b) OT                      (c) NF-planar

Figure 1: Center-outward quantile contours for the Banana distribution in Example 1. Here we include the plot from the reference distribution  $\mathcal{N}(0, I_2)$  and the corresponding contours by passing the reference contours through the transport map estimated by our method (with  $L = 1$ ) and the NF-planar network. We also include axes of the reference distribution to show directional information.

From the plot, we observe that, for our map, all probability mass of  $\mu$  with  $x_1 < 0$  is mapped to the left mode of  $\pi_n$ , while the remaining mass is mapped to the right mode. The quantile contours remain disconnected due to the well-separated components of  $\pi_n$ , demonstrating once again that our quantile contours adapt naturally to the geometric structure of the target distribution. In contrast, while NF-planar is able to generate good approximated samples, its directional information is completely distorted.



(a) OT                      (b) NF-planar

Figure 2: Center-outward quantile contours for the mixture of two bivariate Gaussian example. We use the same reference distribution as in Figure 1(a). We include the contours and sign curves produced by our method and the NF-planar network.

Multivariate center-outward credible regions, whose boundaries are defined by the center-outward quantiles of the posterior distribution  $\pi_n$ , offer a convenient framework for Bayesian exploratory analysis. These regions naturally account for dependencies among parameters and can be used as low-cost tools to reveal specific patterns in the data before engaging in more refined downstream Bayesian inference. We present two applications to demonstrate the effectiveness of the framework.

The first application concerns constructing 95% simultaneous credible intervals  $\{[a_i, b_i]\}_{i=1}^p$  for a  $p$ -dimensional parameter vector  $\theta = (\theta_1, \dots, \theta_p)^T$ , such that

$$\pi_n\left(\bigcap_{i=1}^p \{\theta_i \in [a_i, b_i]\}\right) \geq 95\%. \quad (18)$$

These intervals can serve as an exploratory tool for simultaneously visualizing the uncertainty across multiple parameters, and are especially relevant in settings involving multiple comparisons. Traditional approaches may rely on highest posterior density regions, which are often computationally intensive in high dimensions and difficult to visualize, or Bonferroni-type marginal adjustments, which tend to be overly conservative. In contrast, 95% simultaneous credible intervals can be constructed based on the multivariate center-outward credible region by finding the smallest box  $[a_1, b_1] \times \dots \times [a_p, b_p]$  that can fully contain the 95% credible region. This method is straightforward and computationally scalable to implement, while naturally accommodating multiplicity and dependence across parameters. Specifically, such simultaneous credible intervals can be computed as follows: we generate  $N$  i.i.d. samples uniformly from the 95% quantile sphere of the standard multivariate Gaussian  $\mathcal{N}(0, I_p)$  as the reference distribution  $\mu$ , i.e.  $X^{(j)} \stackrel{iid}{\sim} \text{Unif}(B_p(0, \sqrt{q_{\chi_p^2}(0.95)}}))$ . Here we use  $B_p(0, r)$  to denote a  $p$ -dimensional Euclidean ball centered at the origin, with radius equal to  $r$ , and  $q_{\chi_p^2}(0.95)$  to denote the 0.95 quantile of the chi-squared distribution with  $p$  degrees of freedom. These reference points are then mapped to points in the target parameter space  $\Theta$  via the estimated OT map:  $\hat{\theta}^{(j)} = \hat{T}(X^{(j)})$ . Finally, the desired simultaneous credible intervals can be computed as the coordinate-wise range of these points  $\hat{\theta}^{(j)}$ , that is,  $\{[\min_j \hat{\theta}_i^{(j)}, \max_j \hat{\theta}_i^{(j)}]\}_{i=1}^p$ . These simultaneous credible intervals offer an interpretable and visualizable summary of joint posterior uncertainty. An example of using this approach to assess variable importance in Bayesian logistic regression is presented in Section 5.2.

A second application involves defining and computing a Bayesian analogue of the classical  $p$ -value to assess the plausibility of any multivariate parameter value. The classical  $p$ -value for a given parameter value  $\theta_0$  in the frequentist framework is defined as the probability of observing data, generated under the model  $p(\cdot | \theta_0)$ , that are as extreme or more extreme than the observed data. In a similar way that Bayesian credible intervals quantify uncertainty relative to the posterior distribution of the parameter  $\theta$ , while frequentist confidence intervals quantify uncertainty relative to the sampling distribution of the data, a Bayesian analogue of the  $p$ -value for a parameter  $\theta_0$  can be defined as the posterior probability of parameters that are more extreme than  $\theta_0$ , in contrast to the frequentist  $p$ -value, which is the probability of observing more extreme data under  $\theta_0$ . Fortunately, posterior center-outward quantile contours provide a precise interpretation of extremity in the parameter space and offer a natural basis for defining such “Bayesian  $p$ -values” as a metric to quantify parameter plausibility relative to the posterior distribution.

More specifically, since the optimal transport map preserves the order (rank) of center-outward quantile contours (Chernozhukov et al., 2017), the Bayesian  $p$ -value of a parameter  $\theta_0$  can be computed by evaluating one minus the quantile level corresponding to its preimage  $(T^*)^{-1}(\theta_0)$  under the standard multivariate Gaussian distribution  $\mathcal{N}(0, I_p)$ , which is  $1 - q_{\chi_p^2}^{-1}(\|(T^*)^{-1}(\theta_0)\|_2^2)$ . This application also highlights a distinctive geometric property of the Bayesian OT map  $T^*$ : as the gradient of a convex potential function, it satisfies a form of “multivariate monotonicity”, which ensures the preservation of quantile contour order and enables efficient numerical computation of its inverse,  $(T^*)^{-1}$  (see the following paragraph). Such Bayesian  $p$ -values provide a metric for comparing the plausibility of multiple parameter values. Furthermore, the Bayesian  $p$ -value admits a natural interpretation from the perspective of hypothesis testing for  $H_0 : \theta = \theta_0$  versus  $H_1 : \theta \neq \theta_0$ , as rejecting  $H_0$  when the Bayesian  $p$ -value of  $\theta_0$  falls below a threshold  $\alpha \in (0, 1)$  is equivalent to  $\theta_0$  lying outside the  $100(1 - \alpha)\%$  multivariate center-outward credible region. However, we note that this procedure does not constitute a formal Bayesian test, as Bayesian tests typically rely on Bayes factors, which require placing point prior mass at  $\theta_0$ . Instead, the Bayesian  $p$ -value serves as a fast and interpretable diagnostic tool for identifying parameter values that either align well with, or deviate from, the overall shape of the posterior in Bayesian exploratory analysis.

As mentioned earlier, a key computational advantage of this optimal transport framework for

Bayesian inference is its ability to efficiently compute the reverse OT map  $(T^*)^{-1}$ . This leverages the fact that the  $(T^*)^{-1}$  is related to the conjugate function of its potential  $u^*$  via the identity  $\nabla u^\dagger = (\nabla u^*)^{-1}$ . Therefore, for any posterior sample  $Z$ , its preimage  $X = (T^*)^{-1}(Z)$  can be computed as

$$X = \arg \max_{x \in \mathbb{R}^p} \{ \langle Z, x \rangle - u^*(x) \}.$$

We solve for  $X = (\widehat{T})^{-1}(Z)$  using gradient descent:

$$X^{(t+1)} = X^{(t)} - \alpha_t (\nabla \widehat{u}(X^{(t)}) - Z) = X^{(t)} - \alpha_t (\widehat{T}(X^{(t)}) - Z), \quad t = 0, 1, \dots \quad (19)$$

Since the objective function is convex, as  $\langle Z, x \rangle$  is linear in  $x$  and  $u^*(x)$  is convex, the gradient descent algorithm converges globally (and exponentially if  $u^*$  is strongly convex). This allows us to efficiently compute the pointwise inverse transformation. We denote the solution as  $X = \widehat{R}(Z)$ . Returning to the problem of assessing the plausibility of  $\theta = \theta_0$ , this is equivalently to checking whether  $\|R(\theta_0)\|_2^2 \leq q_{\chi_d^2}(0.95)$ . We illustrate this application in Section 5.2.

The inverse map is also useful for simultaneously comparing or ordering the plausibility of multiple parameter values via OT-derived notion of rankings. For example, we may adopt the center-outward rank  $R_\pm(\cdot)$  following Hallin et al. (2021), which satisfies:

$$R_\pm(Z_1) \geq R_\pm(Z_2) \quad \text{if} \quad \|\widehat{R}(Z_1)\|_2 \geq \|\widehat{R}(Z_2)\|_2.$$

In other words, a point  $Z_1$  is ranked higher than  $Z_2$  if its preimage under the inverse map is closer to the origin in the reference distribution. This is equivalent to saying that  $Z_1$  belongs to a lower quantile contour than  $Z_2$ . Figure 3 visualizes these ranks for 10 random draws from the banana distribution in Example 1. The reverse-mapped points in the reference Gaussian clearly preserve the intended ordering structure.

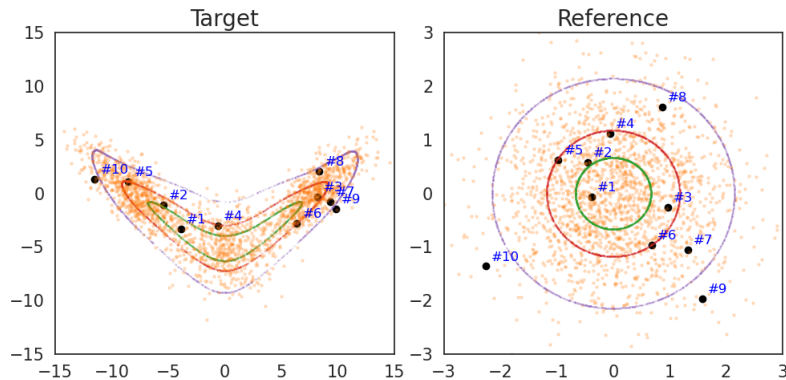


Figure 3: Center-outward ranks for 10 random draws  $Z_i$  from the banana distribution, and their corresponding locations  $\hat{h}(Z_i) = (\hat{T})^{-1}(Z_i)$  in the reference distribution.

## 5 Simulation Studies

In this section, we compare our approach with two alternative transport-based methods, transport Monte Carlo (TMC) by Duan (2021) and normalizing flow (Rezende and Mohamed, 2015) with planar transformers (NF-planar). Here we provide a brief summary of these two methods. TMC approximates the conditional density using a mixture of transport maps, where each map only involves location-scale changes. NF applies a sequence of invertible and differentiable transformations to map the reference distribution to the target distribution. For NF-planar, it uses the planar transformation, which takes the form  $f(x) = x + \alpha\varphi(\langle a, x \rangle + b)$ , in each layer and it is relatively cheap to compute. The detailed configurations of our method, TMC and NF-planar for each simulation example are provided in Section A.4.

### 5.1 Mixture of Gaussian distributions

In this experiment, we examine the performance of different methods on multi-modal continuous distributions, specifically mixtures of  $K$  multivariate normals in  $\mathbb{R}^d$ . The target distribution is defined as  $\pi_n = \frac{1}{K} \sum_{k=1}^K N(m_k, \Sigma_k)$ , where  $\{m_k, \Sigma_k\}_{k=1}^K$  are assumed to be known. We consider 6 combinations of  $d$  and  $K$ , where  $d \in \{5, 10, 20\}$  and  $K \in \{3, 10\}$ . The cluster means  $\{m_k\}_{k=1}^K$  are generated from uniform distribution  $\text{Unif}[-10, 10]$  and the covariance matrices  $\Sigma_k$  for  $k \in [K]$  are defined as  $(\Sigma_k)_{ij} = \rho_k^{|i-j|}$  with  $\rho_k = (-1)^k 0.5$ . We use the standard Gaussian distribution as our reference distribution for this example.

Both NF and TMC struggle with learning multi-modal distributions. NF-planar is mainly

designed for continuous target distribution since it is constructed with continuous functions, therefore it does not work well when the target distribution has well-separated modes, especially in high-dimensional settings. Meanwhile, even though TMC incorporates a multinomial mixture weight, but its transport plan is not specifically optimized for multi-modal characteristics targets. As a result, it is computationally costly for TMC to approximate target distributions with multiple modes.

In contrast, our transport map in (11) is explicitly designed for multi-modal target distributions by leveraging the structure in Lemma 3. Specifically, we choose  $L = 3$  when  $K = 3$  and  $L = 32$  when  $K = 10$ . The modes are close to each other and hard to distinguish when  $K = 10$ , therefore we choose  $L = 32$  to add stability to our transport map. We set  $M_\ell = 16, 32, 64$  for  $\ell \in [L]$  when  $d = 5, 10, 20$ , respectively.

(d, K)	Benchmark	Our method	NF-planar	TMC
(5, 3)	0.859	1.838	3.547	2.420
(5, 10)	1.547	2.671	4.393	6.560
(10, 3)	2.213	3.923	6.463	14.696
(10, 10)	3.039	5.562	10.310	12.683
(20, 3)	3.901	10.287	9.979	21.694
(20, 10)	4.769	11.334	17.546	24.954

Table 1: 2-Wasserstein distance between 10,000 samples from target distribution and each method at different combinations of  $d$  and  $K$ .

Table 1 reports the 2-Wasserstein distances between 10 000 samples from the target distribution and those generated by each method. We also include the benchmark distance between two independent sets of 10 000 samples from the true target distribution to measure sampling variation. We observe that our transport map achieves the smallest distance among all methods at different  $d$  and  $K$ , except the case of  $d = 20, K = 3$ . The performance gap between our method and the other two methods grows as  $K$  or  $d$  is larger, since it is harder for NF and TMC to identify all modes and capture the variability of the distribution while our method can handle both effectively.

Figure 4 provides a visual comparison of samples generated by each method for  $d = 20$  and  $K = 10$ . Our transport map with  $L = 32$  and  $M_\ell = 64$  for  $l \in [L]$  has the best performance that it accurately captures all modes and preserves the correct spread of each cluster. In contrast, TMC only identifies only 4 modes and NF-planar does not capture the shape of all clusters correctly,

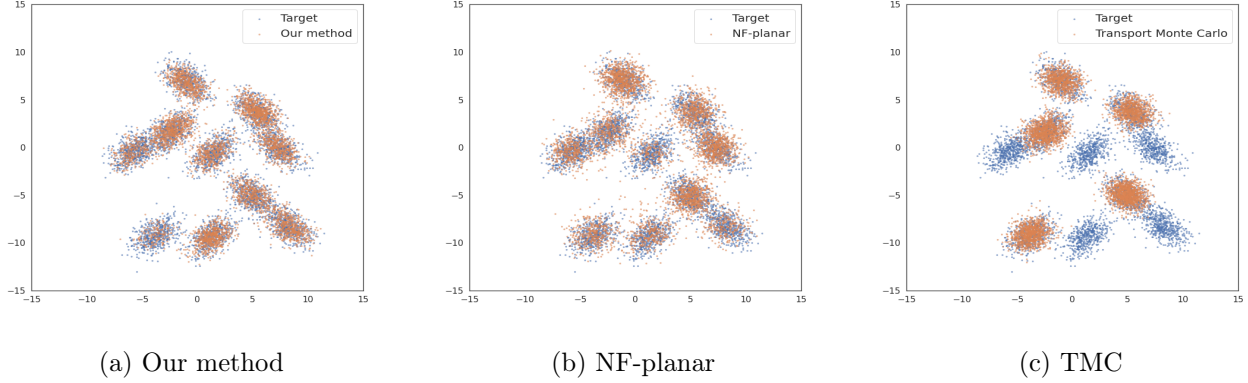


Figure 4: Comparison of draws generated from the target distribution and different approximate methods when  $d = 20$  and  $K = 10$ .

suggesting loss of correlation information.

## 5.2 Bayesian logistic regression

In this simulation study, we investigate the performance of our method on a continuous and uni-modal distribution. We consider the Bayesian logistic regression model, which has been long been a challenging problem due to the complicated form of the binomial likelihood. A commonly used strategy to enable conjugate updating is the Polya-Gamma data augmentation (Polson et al., 2013), but its implementation can be rather complicated. Our method offers a simpler and more direct alternative.

Assume that we have  $n$  binary responses  $\{y_1, y_2, \dots, y_n\}$  taking values in  $\{0, 1\}$  and their  $p$ -dimensional covariates  $\{x_1, x_2, \dots, x_n\} \subseteq \mathbb{R}^p$ , the posterior distribution of the regression coefficient  $\beta \in \mathbb{R}^p$  is

$$\pi_n(\beta \mid \mathbf{x}, \mathbf{y}) \propto \underbrace{\prod_{i=1}^n \frac{(e^{x_i^T \beta})^{y_i}}{1 + e^{x_i^T \beta}}}_{\text{likelihood}} \times \underbrace{\pi(\beta)}_{\text{prior}},$$

where  $\mathbf{y} = (y_1, y_2, \dots, y_n)^T$ ,  $\mathbf{x} = (x_1, x_2, \dots, x_n)^T$  and we consider a non-informative prior  $\beta \sim N(0, \sigma^2 I_p)$  with  $\sigma = 10$ .

For the simulated dataset, we set  $n = 1000$  and  $p = 10$ . The entries of the ground truth  $\beta$  are generated from uniform distribution  $\text{Unif}[-1, 1]$ . We generate  $x_i \in \mathbb{R}^p$  for  $i = 1, \dots, N$  from Gaussian distribution  $N(0, \Sigma)$  with Toeplitz covariance matrix  $\Sigma_{ij} = \rho^{|i-j|}$ , where  $\rho$  is chosen from

$\{0.1, 0.3, 0.5, 0.7, 0.9\}$ . For our method, since the posterior  $\pi_n$  is unimodal, it suffices to set  $L = 1$  in our approximation family (11). In particular, since  $n$  is much bigger than  $p$  in this example, we consider using the simple linear transport map discussed in (15) to approximate the posterior, referred as OT\_linear.

We use the Gibbs sampler as a benchmark as direct sampling from  $\pi_n$  is infeasible. The quality of different samplers is assessed using two metrics: (1) the difference ratio of 95% credible intervals (CIs); (2) 2-Wasserstein distance between 500 draws from the Gibbs sampler and the transport-based methods. All metrics are averaged over 100 repeated experiments. For the 95% CIs, we obtain 500 draws from each sampler and construct the marginal 95% credible interval for each parameter. The difference ratio for the CIs is defined as  $|I_1 \oplus I_2| / |I_1|$ , where  $I_1$  is the Gibbs sampler interval,  $I_2$  is the length of the transport map method interval and  $I_1 \oplus I_2 = (I_1 \cup I_2) \setminus (I_1 \cap I_2)$ . For the 2-Wasserstein distance, we report the standardized 2-Wasserstein distance to adjust for variability across different  $\rho$ . Basically we divide each parameter by its standard deviation calculated from the Gibbs sampler draws, then compute the 2-Wasserstein distance on the standardized parameters and average over 10 parameters. The results under different correlation strength  $\rho$  are summarized in Figure 5.

From Figure 5a, we observe that our methods consistently perform best across all values of  $\rho$ , while TMC performs significantly worse in terms of both credible intervals and predictive intervals. It is also worth noting that the difference between our map estimated using the regular convex unit construction with  $L = 1$  (OT) and the much simpler linear map (OT\_linear) in (15) is minimal. This provides empirical support for the effectiveness of the linear approximation in (15), particularly when the sample size  $n$  is large.

**Exploratory analysis using OT-derived quantiles.** In addition to the comparison with the Gibbs sampler, which shows that our method consistently yields the smallest approximation error, we present another example to illustrate the inferential advantage of our approach described in Section 4.3 for exploratory analysis involving multiple parameters.

We consider a sparse regression setting with  $\beta = (2, 0, 4, 0, 3, 0, -1, 0, 1, 0)^T$  and introduce moderate correlation among predictors by setting  $\rho = 0.5$ . This induces dependency among the posterior marginals of the coefficients  $\hat{\beta}_i$ , which can complicate interpretation when relying solely

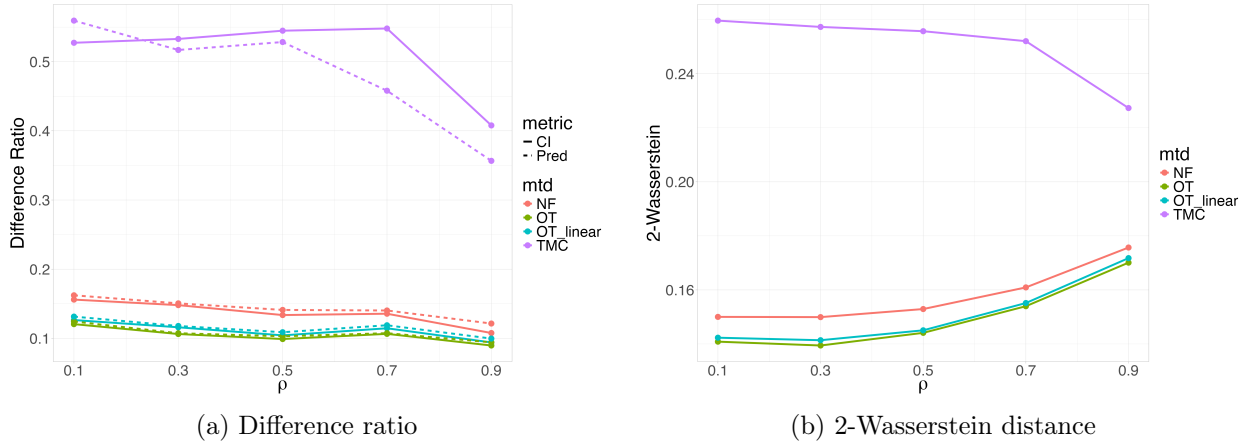


Figure 5: Difference ratio of 95% credible intervals for parameters and 95% prediction intervals of new data points, and the standardized 2-Wasserstein distance for posterior distributions under transport map methods compared with the Gibbs posterior.

on marginal summaries. In such cases, simultaneous credible intervals based on the center-outward quantile regions in Section 4.3 provide a way to visualize and assess joint uncertainty while capturing dependencies among parameters.

Recall that our method constructs an approximate 95% simultaneous credible intervals by identifying the smallest axis-aligned box that encloses the 95% center-outward credible region, as described in Section 4.3. For exploratory purposes, we can assess how each coefficient compares to zero by checking whether zero lies within its corresponding interval. This visualization provides an interpretable overview of parameter relevance that accounts for joint dependence and familywise error control, helping to flag potentially interesting variables for further investigation. We provide a close look at the posterior distribution in Figure 6.

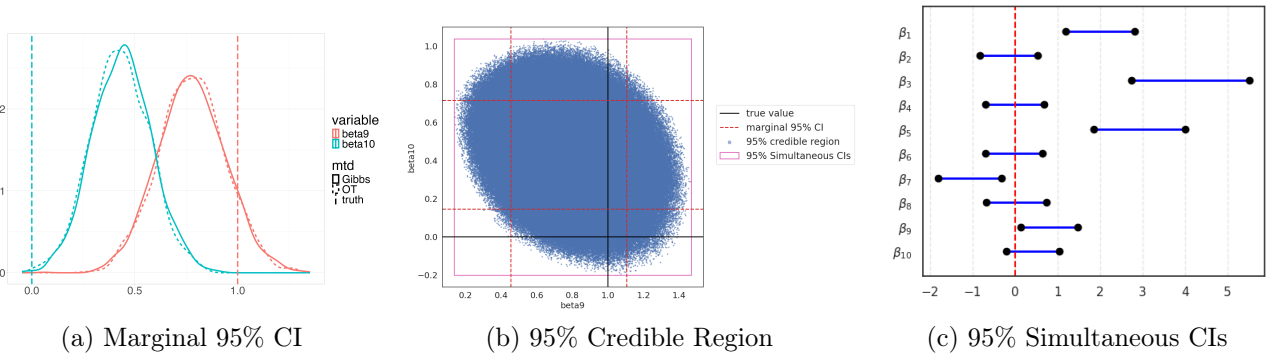


Figure 6: Posterior summary for  $(\beta_9, \beta_{10})$  and simultaneous credible intervals for all  $\beta_j$ 's. Here we include: (a) marginal density of  $\beta_9$  and  $\beta_{10}$  produced by Gibbs posterior and our method (OT); (b) the 95% credible region by OT (projected onto  $(\beta_9, \beta_{10})$ ); and (c) all 95% simultaneous credible intervals (CIs)

As shown in Figure 6a, the marginal posterior distributions obtained from our method closely match those from the Gibbs sampler. Both approaches yield marginal 95% credible intervals for  $\beta_{10}$  that exclude zero. However, examining the joint distribution of  $(\beta_9, \beta_{10})$  in Figure 6b reveals a negative correlation between the two, which is captured by the OT-based credible region. This structure suggests that the marginal view may overstate the evidence against  $\beta_{10} = 0$ , while the joint credible region offers a more nuanced interpretation. Such insights may guide more careful follow-up testing procedures, especially in settings with strong parameter dependence. In Figure 6c, we provide a visualization of all 95% simultaneous credible intervals and 5 out of 10 intervals contain zero. This exploratory analysis suggests that incorporating variable selection for parsimonious modeling, for example, through using sparsity inducing priors on the regression coefficients, might be useful to improve the predictive and inference performance.

For multivariate hypotheses involving multiple parameters, such as exploring the plausibility of the null model with  $\beta = (0, 0, \dots, 0)^T$ , it can be informative to examine the preimage of the hypothesized value under the OT map. In this example, we find the preimage is located at  $(-27.0, 4.1, -50.6, -2.3, -37.9, 10.9, 16.3, 16.2, -12.1, -3.3)^T$  with an  $\ell_2$ -norm of 74.5. For comparison, the radius corresponding to the 95% quantile region of a  $\chi_{10}^2$  distribution is  $q_{\chi_{10}^2}(0.95) = 18.3$ . Furthermore, we can compute the ‘‘Bayesian p-value’’ of this preimage as  $1 - q_{\chi_{10}^2}^{-1}(74.5^2) < 2.22 \times 10^{-16}$ , i.e, smaller than the minimal machine precision. This suggests that the joint configuration  $\beta = 0$  is extremely unlikely under the posterior distribution. Although not a formal test, this approach offers a computationally efficient way to assess how compatible a specific multivariate parameter value is with the joint posterior structure, and may serve as a useful tool for model checking and/or comparison in Bayesian exploratory analysis.

### 5.3 Gaussian mixture models

In this subsection, we evaluate the performance of our ‘‘mean-field’’ transport map on Bayesian Gaussian mixture model with  $K = 3$  mixture components, as discussed in Section 4.2. The goal is to assess how well our method approximates the posterior distribution of both latent variables  $\{c_i\}$  and cluster means  $\{\mathbf{m}_k\}$ .

We generate  $n = 300$  samples  $Z^{(n)} = \{Z_1, Z_2, \dots, Z_n\}$  in  $p = 2$  dimensions and their latent

variables  $\{c_1, c_2, \dots, c_n\}$  are uniformly generated from the  $K$  components. For the cluster means, we consider  $\{m_1 = (-\Delta/2, 0)^T, m_2 = (0, \Delta)^T, m_3 = (\Delta/2, 0)^T\}$  where  $\Delta \in \{2, 4, 6\}$  controls the separation between clusters. When  $\Delta$  is small, the clusters are closer to each other and the problem becomes harder. Then given the latent variable  $c_i$ , the observations are drawn from  $Z_i | c_i \sim N(m_{c_i}, I_2)$ . We set the prior for cluster means as  $m_k \sim \mathcal{N}(0, 10^2 I_2)$  for every  $k = 1, \dots, K$ .

Similar to Section 5.2, we use the Gibbs sampler as a benchmark. Given the large latent space, TMC is computationally infeasible, so we only compare our method to NF-planar. To evaluate the performance of our transport map, we generate 500 posterior samples of latent variables  $\{c_i\}$  and means of clusters  $\{m_k\}$  from both our method and the Gibbs sampler. We compute the total variation distance between draws on each latent variable  $c_i$ , and take the average over all 300  $c_i$ 's. For the cluster mean parameters  $\{m_k\}$ , we compute the empirical 2-Wasserstein distance. We compare our method with NF-planar. Since NF-planar does not produce posteriors for latent variables, we are only computing its performance on the mean parameters  $\{m_k\}$ . All metrics are then further averaged over 100 repeated experiments and the results are reported in Table 2. For this example, our performance in estimating cluster means is comparable with NF-planar. However, compared to NF-planar which integrates out the latent variables in their approximation, our method can estimate both latent variables  $c_i$  and the mean parameters  $m_k$  at the same time so our posterior maintains better interpretability.

	$\Delta = 2$		$\Delta = 4$		$\Delta = 6$	
	Ours	NF-planar	Ours	NF-planar	Ours	NF-planar
Latent variables	0.021	-	0.010	-	0.015	-
$m_1$	0.048	0.045	0.018	0.016	0.025	0.022
$m_2$	0.057	0.051	0.021	0.019	0.026	0.023
$m_3$	0.055	0.053	0.019	0.017	0.026	0.024

Table 2: Average total variation distance for latent variables and 2-Wasserstein distance for cluster means over 100 replications for our method and NF-planar. The probability mass function of the latent variable is computed in closed form instead of using soft-max approximation.

## 6 Empirical Analysis on the *yeast* Dataset

In this section, we evaluate the performance of our method on the yeast dataset (Elisseeff and Weston, 2001). The dataset contains 2,417 genes, each with 103 covariates and 14 gene functional

classes. Each functional class defines an independent binary classification task. In our analysis, we focus on the first gene functional class and model the problem using Bayesian logistic regression.

We begin by pre-screening covariates, retaining only those with an absolute correlation of at least 0.1 with the class label. This filtering step results in 24 covariates. We then apply a generalized linear model (GLM) for standard logistic regression and use an MCMC implementation for Bayesian logistic regression. Our method is compared with two alternatives: NF-planar and TMC. We assess performance from two perspectives: uncertainty quantification and variable selection. For variable selection, a covariate is considered significant if its marginal 95% credible interval (or confidence interval) does not include zero. Since the true model is unknown, we use the MCMC posterior as the benchmark.

When trained on the full dataset, both GLM and MCMC identify the same 10 significant covariates (including the intercept) at a 5% significance level. Among the transport map methods, our approach selects exactly the same covariates as MCMC. Note that we also check the significance of covariates using the 95% simultaneous credible intervals we show in Section 5.2 and we find only 7 covariates significant, suggesting strong correlation among covariates. In contrast, NF-planar misses one covariate, and TMC selects two additional covariates not selected by MCMC. To evaluate predictive performance, we split the dataset into training and testing subsets, with 70% of the data used for training. Our method achieves a test accuracy of 76.9%, slightly outperforming NF-planar (76.4%) and TMC (76.8%), and comparable to the MCMC-based method (76.7%).

We further analyze uncertainty quantification by comparing the 95% credible interval length difference ratios between the transport-based methods and MCMC, as described in Section 5.2. The results for the 10 significant variables are shown in Table 3. For most variables, the credible intervals produced by our method are the closest in length to those from MCMC, further supporting its reliability.

To assess robustness, we repeat the variable selection process 100 times using different train-test splits. In Table 4, we report the average number of over-selected and under-selected variables compared to MCMC, which selects an average of 10.2 significant variables. Over-selection refers to variables selected by the transport method but not by MCMC, while under-selection refers to variables selected by MCMC but missed by the transport method. From Table 4, we observe that

	Intercept	Att3	Att34	Att58	Att66
Our method	0.026	0.021	0.020	0.014	0.002
NF-planar	0.018	0.052	0.090	0.035	0.050
TMC	0.012	0.026	0.125	0.009	0.025
	Att79	Att88	Att89	Att96	Att102
Our method	0.004	0.020	0.025	0.007	0.019
NF-planar	0.046	0.037	0.033	0.020	0.005
TMC	0.063	0.063	0.044	0.065	0.011

Table 3: Difference ratio of 95% credible intervals between transport map methods and the MCMC posterior for the 10 significant variables selected by MCMC.

our method consistently yields the closest variable selection results to MCMC. This is consistent with the fact that its credible intervals are also the most similar to those from MCMC. These results highlight that our method is a reliable and computationally efficient alternative for Bayesian logistic regression, offering both accurate uncertainty quantification and robust variable selection.

	Our method	NF-planar	TMC
#under-select	0.19	0.27	0.22
#over-select	0.27	0.53	0.63

Table 4: Average number of under-select and over-select significant variables from transport map methods compared with MCMC over 100 repetitions.

## 7 Discussion

In this paper, we propose an efficient sampler for posterior distributions with unknown normalizing constants. Our goal is to construct a transport map that pushforwards a simple reference distribution to the target posterior distribution. Once the map is learned, independent samples from the posterior can be generated at negligible computational cost. We obtain the map by optimizing the Kullback–Leibler (KL) divergence between the transported distribution and the target distribution, a formulation that does not require knowledge of the normalizing constant. Similar ideas have been explored in previous works such as Kim et al. (2013); El Moselhy and Marzouk (2012).

The key innovation of our method lies in the structural constraint imposed on the pre-specified transport map class  $\mathcal{T}$ , inspired by optimal transport theory. This structured map class ensures unique recovery of the optimal transport map in the Monge problem, significantly reducing computational complexity. Moreover, the structural constraint enables novel applications in multivariate

ranks and quantiles, offering strong potential for Bayesian exploratory analysis and visualization.

Several promising avenues for future research remain. One interesting direction is to relax the invertibility assumption in Lemma 1 and develop new methods for estimating transport maps that are better aligned with the geometric structures of the Wasserstein space. For instance, if the target distribution lies on a low-dimensional manifold (Arjovsky et al., 2017), it may be beneficial to use a  $p^*$ -dimensional reference distribution with  $p^* < p$ , where  $p^*$  matches the intrinsic rather than the observed dimension. This approach could further reduce computational complexity and enhance the interpretability of the generative model.

From a theoretical standpoint, it would be valuable to conduct an error analysis of our model and, more broadly, of general Wasserstein gradient flows. For example, Theorem 4.1 in Kingma and Ba (2014) provides convergence guarantees for an efficient optimization algorithm. Such results could be integrated with existing error bounds for training generative models, such as those in Mei et al. (2018), to yield a more refined upper bound.

Finally, we highlight a potential application of our framework. Graphical models (Wainwright and Jordan, 2008) are a central topic in Bayesian machine learning. While this work has primarily focused on models with a single hierarchy, many widely used models involve multiple hidden layers (Blei and Lafferty, 2007). Previous research (Chen et al., 2020; Akagi et al., 2020; Haasler et al., 2021) has studied the discrete case, where the target distribution is an empirical distribution arising from a graphical model. However, the continuous and mixed-variable cases remain underexplored. Our method provides a new perspective on addressing these more complex scenarios.

## References

- Y. Akagi, Y. Tanaka, T. Iwata, T. Kurashima, and H. Toda. Probabilistic optimal transport based on collective graphical models. *arXiv preprint arXiv:2006.08866*, 2020.
- B. Amos, L. Xu, and J. Z. Kolter. Input convex neural networks. In *International Conference on Machine Learning*, pages 146–155. PMLR, 2017.

- M. Arjovsky, S. Chintala, and L. Bottou. Wasserstein generative adversarial networks. In *International conference on machine learning*, pages 214–223. PMLR, 2017.
- G. Biau, B. Cadre, M. Sangnier, and U. Tanielian. Some theoretical properties of GANS. *The Annals of Statistics*, 48(3):1539 – 1566, 2020. doi: 10.1214/19-AOS1858. URL <https://doi.org/10.1214/19-AOS1858>.
- D. M. Blei and J. D. Lafferty. A correlated topic model of science. *The Annals of Applied Statistics*, 1(1):17–35, 2007.
- D. M. Blei, A. Kucukelbir, and J. D. McAuliffe. Variational inference: A review for statisticians. *Journal of the American statistical Association*, 112(518):859–877, 2017.
- Y. Brenier. Polar factorization and monotone rearrangement of vector-valued functions. *Communications on Pure and Applied Mathematics*, 44(4):375–417, 1991.
- A. Brock, J. Donahue, and K. Simonyan. Large scale gan training for high fidelity natural image synthesis, 2018.
- L. A. Caffarelli. Boundary regularity of maps with convex potentials. *Communications on Pure and Applied Mathematics*, 45(9):1141–1151, 1992a.
- L. A. Caffarelli. The regularity of mappings with a convex potential. *Journal of the American Mathematical Society*, 5(1):99–104, 1992b.
- B. Chen, G. Bécigneul, O.-E. Ganea, R. Barzilay, and T. Jaakkola. Optimal transport graph neural networks. *arXiv preprint arXiv:2006.04804*, 2020.
- V. Chernozhukov, A. Galichon, M. Hallin, and M. Henry. Monge–kantorovich depth, quantiles, ranks and signs. *The Annals of Statistics*, 45(1):223–256, 2017.
- M. Cuturi. Sinkhorn distances: Lightspeed computation of optimal transport. In *Proceedings of the 26th International Conference on Neural Information Processing Systems - Volume 2, NIPS’13*, page 2292–2300, Red Hook, NY, USA, 2013. Curran Associates Inc.

- G. De Philippis and A. Figalli. The Monge–Ampère equation and its link to optimal transportation. *Bulletin of the American Mathematical Society*, 51(4):527–580, 2014.
- L. L. Duan. Transport Monte Carlo: High-accuracy posterior approximation via random transport. *Journal of the American Statistical Association*, (just-accepted):1–30, 2021.
- D. B. Dunson, N. Pillai, and J.-H. Park. Bayesian density regression. *Journal of the Royal Statistical Society: Series B (Statistical Methodology)*, 69(2):163–183, 2007.
- T. A. El Moselhy and Y. M. Marzouk. Bayesian inference with optimal maps. *Journal of Computational Physics*, 231(23):7815–7850, 2012.
- A. Elisseeff and J. Weston. A kernel method for multi-labelled classification. In *Proceedings of the 14th International Conference on Neural Information Processing Systems: Natural and Synthetic*, NIPS’01, page 681–687, Cambridge, MA, USA, 2001. MIT Press.
- R. Flamary, N. Courty, A. Gramfort, M. Z. Alaya, A. Boisbunon, S. Chambon, L. Chapel, A. Corenflos, K. Fatras, N. Fournier, L. Gautheron, N. T. Gayraud, H. Janati, A. Rakotomamonjy, I. Redko, A. Rolet, A. Schutz, V. Seguy, D. J. Sutherland, R. Tavenard, A. Tong, and T. Vayer. Pot: Python optimal transport. *Journal of Machine Learning Research*, 22(78):1–8, 2021. URL <http://jmlr.org/papers/v22/20-451.html>.
- A. Gelman, J. B. Carlin, H. S. Stern, D. B. Dunson, A. Vehtari, and D. B. Rubin. *Bayesian data analysis*. CRC press, 2013.
- G.-L. Geuken, P. Kurzeja, D. Wiedemann, and J. Mosler. Input convex neural networks: universal approximation theorem and implementation for isotropic polyconvex hyperelastic energies. *arXiv preprint arXiv:2502.08534*, 2025.
- I. J. Goodfellow, J. Pouget-Abadie, M. Mirza, B. Xu, D. Warde-Farley, S. Ozair, A. Courville, and Y. Bengio. Generative adversarial networks, 2014.
- I. Haasler, R. Singh, Q. Zhang, J. Karlsson, and Y. Chen. Multi-marginal optimal transport and probabilistic graphical models. *IEEE Transactions on Information Theory*, 67(7):4647–4668, 2021.

- M. Hallin, E. del Barrio, J. Cuesta-Albertos, and C. Matrán. Distribution and quantile functions, ranks and signs in dimension  $d$ : A measure transportation approach. *Annals of Statistics*, 49(2): 1139–1165, 2021.
- M. Hoffman, P. Sountsov, J. V. Dillon, I. Langmore, D. Tran, and S. Vasudevan. Neutralizing bad geometry in Hamiltonian Monte Carlo using neural transport. *arXiv preprint arXiv:1903.03704*, 2019.
- F. Huszár. Variational inference using implicit distributions. *arXiv preprint arXiv:1702.08235*, 2017.
- H. Ishwaran and J. S. Rao. Spike and slab variable selection: frequentist and bayesian strategies. *The Annals of Statistics*, 33(2):730–773, 2005.
- A. Jasra, C. C. Holmes, and D. A. Stephens. Markov Chain Monte Carlo Methods and the Label Switching Problem in Bayesian Mixture Modeling. *Statistical Science*, 20(1):50 – 67, 2005.
- A. Katsevich. Improved dimension dependence in the Bernstein von Mises theorem via a new Laplace approximation bound. *arXiv preprint arXiv:2308.06899*, 2023.
- M. Katzfuss and F. Schäfer. Scalable bayesian transport maps for high-dimensional non-gaussian spatial fields. *arXiv preprint arXiv:2108.04211*, 2021.
- S. Kim, R. Ma, D. Mesa, and T. P. Coleman. Efficient bayesian inference methods via convex optimization and optimal transport. In *2013 IEEE International Symposium on Information Theory*, pages 2259–2263. IEEE, 2013.
- D. P. Kingma and J. Ba. Adam: A method for stochastic optimization. *arXiv preprint arXiv:1412.6980*, 2014.
- J. Kitagawa and R. McCann. Free discontinuities in optimal transport. *Archive for Rational Mechanics and Analysis*, 232(3):1505–1541, 2019.
- L. M. Le Cam and G. L. Yang. *Asymptotics in statistics: some basic concepts*. Springer Science & Business Media, 2000.

- Y. Li, K. Swersky, and R. Zemel. Generative moment matching networks, 2015.
- R. Y. Liu. On a notion of data depth based on random simplices. *The Annals of Statistics*, pages 405–414, 1990.
- A. Magnani and S. P. Boyd. Convex piecewise-linear fitting. *Optimization and Engineering*, 10:1–17, 2009.
- R. J. McCann. Existence and uniqueness of monotone measure-preserving maps. *Duke Mathematical Journal*, 80(2):309–324, 1995.
- S. Mei, A. Montanari, and P.-M. Nguyen. A mean field view of the landscape of two-layer neural networks. *Proceedings of the National Academy of Sciences*, 115(33):E7665–E7671, 2018.
- S. Mohamed and B. Lakshminarayanan. Learning in implicit generative models. *arXiv preprint arXiv:1610.03483*, 2016.
- M. Panov and V. Spokoiny. Finite sample Bernstein–von Mises theorem for semiparametric problems. *Bayesian Analysis*, 10(3):665–710, 2015.
- N. G. Polson, J. G. Scott, and J. Windle. Bayesian inference for logistic models using Pólya–Gamma latent variables. *Journal of the American statistical Association*, 108(504):1339–1349, 2013.
- L. R. Rabiner. A tutorial on hidden markov models and selected applications in speech recognition. *Proceedings of the IEEE*, 77(2):257–286, 1989.
- D. Rezende and S. Mohamed. Variational inference with normalizing flows. In *International Conference on Machine Learning*, pages 1530–1538. PMLR, 2015.
- F. Santambrogio. Optimal transport for applied mathematicians. *Birkäuser, NY*, 55(58-63):94, 2015.
- I. Tolstikhin, O. Bousquet, S. Gelly, and B. Schoelkopf. Wasserstein auto-encoders, 2019.
- J. W. Tukey. Mathematics and the picturing of data. In *Proceedings of the international congress of mathematicians*, volume 2, pages 523–531. Vancouver, 1975.

- A. van den Oord, S. Dieleman, H. Zen, K. Simonyan, O. Vinyals, A. Graves, N. Kalchbrenner, A. Senior, and K. Kavukcuoglu. Wavenet: A generative model for raw audio, 2016.
- A. W. van der Vaart. *Asymptotic statistics*, volume 3. Cambridge university press, 2000.
- C. Villani. *Topics in optimal transportation*. Number 58. American Mathematical Soc., 2003.
- C. Villani. *Optimal transport: old and new*, volume 338. Springer Science & Business Media, 2008.
- M. J. Wainwright and M. I. Jordan. Graphical models, exponential families, and variational inference. *Foundations and Trends<sup>®</sup> in Machine Learning*, 1(1–2):1–305, 2008.
- Y. Yang, D. Pati, and A. Bhattacharya.  $\alpha$ -variational inference with statistical guarantees. *The Annals of Statistics*, 48(2):886–905, 2020.
- Y. Zhang and Y. Yang. Bayesian model selection via mean-field variational approximation. *Journal of the Royal Statistical Society Series B: Statistical Methodology*, 2024.
- S. Zhao, J. Song, and S. Ermon. Infovae: Information maximizing variational autoencoders, 2018.

# Appendices

The supplementary material is organized as follows. In Section A, we describe additional computational details related to the algorithms and numerical studies discussed in the main paper. In Section B, we give further details on some of the key algorithms. Finally, in Section C, we provide all proofs of the lemmas and theorems presented in the main paper.

## A Computational Details

### A.1 Computational Details of Gradients and Jacobians

While automatic differentiation packages help us avoid manually coding backpropagation, certain gradients are still computed by hand. For example, the baseline appears as an input to the exact or approximate objective function in Lemma 1. First, for a convex basis unit  $u_i(x) = f(x; \alpha_i, \beta_i, w_i, v_i)$ , we can compute the derivative as

$$\nabla u_i(x) = \varphi_i(\langle \alpha_i, x \rangle + w_i) \alpha_i + \beta_i. \quad (20)$$

The exact derived transform and Jacobian matrix of map in (21) follow from Lemma 5.

### A.2 Computation Details of Lemma 6

We first generate  $N_x$  samples  $\{x_1, x_2, \dots, x_{N_x}\}$  i.i.d. from  $\mu$ , and then compute the corresponding transformed variables  $\{\theta_1, \theta_2, \dots, \theta_{N_x}\}$  through transport map  $T$ , where  $\theta_i = (\tau_i, \zeta_i)$  with  $\zeta_i = \nabla \phi_{\tau_i}(X_i^{(2)})$  and

$$\tau_i = \arg \max_{k \in [K]} \left\{ \langle x_i^{(1)}, b_k \rangle + \phi_k(x_i^{(2)}) \right\}, \quad \text{for } i = 1, 2, \dots, N_x.$$

To approximate generally intractable conditional probability  $\mathbb{P}(\tau_i \mid x_i^{(2)})$  in objective (13) for each sample  $(\tau_i, x_i^{(2)})$ , we apply the Monte Carlo method again. We generate  $N_z$  samples  $\{z_{i,1}^{(1)}, z_{i,2}^{(1)}, \dots, z_{i,N_z}^{(1)}\}$  i.i.d. from  $\mu_1$  for each sample  $x_i^{(2)}$ , and computing the transported variables

$\{w_{i,1}^{(1)}, w_{i,2}^{(1)}, \dots, w_{i,N_z}^{(1)}\}$  as

$$w_{i,j}^{(1)} = \arg \max_{k \in [K]} \left\{ \langle z_{i,j}^{(1)}, b_k \rangle + \phi_k(x_i^{(2)}) \right\}, \quad \text{for } j = 1, 2, \dots, N_z.$$

Then probability  $\mathbb{P}(\tau_i | x_i^{(2)})$  can be approximated by the empirical distribution,

$$\widehat{\mathbb{P}}(\tau_i | x_i^{(2)}) := \frac{1}{N_z} \sum_{j=1}^{N_z} \mathbb{1}_{\{w_{i,j}^{(1)} = \tau_i\}} \approx \frac{1}{N_z} \sum_{j=1}^{N_z} W_{i,j}(\tau_i),$$

where  $W_{i,j}$  denotes the softmax approximation of the indicator function, i.e.,

$$W_{i,j}(\tau_i) = \frac{\exp\left(\gamma(\langle z_{i,j}^{(1)}, b_{\tau_i} \rangle + \phi_{\tau_i}(x_i^{(2)}))\right)}{\sum_{k \in [K]} \exp\left(\gamma(\langle z_{i,j}^{(1)}, b_k \rangle + \phi_k(x_i^{(2)}))\right)},$$

with  $\gamma > 0$  a tuning parameter. Here we use the softmax approximation to make the objective function differentiable, so that efficient gradient descent algorithms can be applied to the optimization. In practice, we may reuse the samples  $\{x_1^{(1)}, x_2^{(1)}, \dots, x_{N_x}^{(1)}\}$  when generating the  $\tau_i$ 's as  $\{z_{i,1}^{(1)}, z_{i,2}^{(1)}, \dots, z_{i,N_z}^{(1)}\}$  to facilitate computational efficiency and reduce space complexity.

### A.3 Computation in Gaussian mixture models

Here we describe the optimization details of the transport map  $T$  in Section 4.2. According to Lemma 6, we first generate  $N$  samples  $\{x_1, x_2, \dots, x_N\} \in \mathbb{R}^{n(K-1)+Kd}$  i.i.d. from the reference distribution  $\mu$ . Then, the transport map  $T$  will map the samples to  $\{\xi_1, \xi_2, \dots, \xi_n\}$ . To approximate the expectation in Lemma 6, we need to calculate the log-likelihood of the posterior distribution for each sample  $\xi_i := (\xi_i^{(1)}, \xi_i^{(2)})$ , where  $\xi_i^{(1)} := (\xi_{i,1}^{(1)}, \dots, \xi_{i,n}^{(1)}) \in \mathbb{R}^{n(K-1)}$  corresponds to the latent variables and  $\xi_i^{(2)} = (\xi_{i,1}^{(2)}, \dots, \xi_{i,K}^{(2)}) \in \mathbb{R}^{Kd}$  corresponds to the concatenated vector  $\zeta$  of cluster means.

In the GMM model, the log-likelihood of the posterior of  $(\tau, \zeta)$  can be expressed as

$$\log p(\tau, \zeta | Z^{(n)}) = \sum_{k=1}^K \log p(m_k) + \sum_{i=1}^N \log p(c_i) + \sum_{i=1}^N \log p(Z_i | c_i, \zeta)$$

$$\begin{aligned} &\propto \sum_{k=1}^K \left[ -\frac{1}{2\sigma^2} (m_k - m_0)^T (m_k - m_0) \right] - n \log K \\ &\quad + \sum_{i=1}^N \left[ -\frac{1}{2\lambda^2} (Z_i - m_{c_i})^T (Z_i - m_{c_i}) \right]. \end{aligned}$$

Then, for each transported sample  $\xi_i \in \mathbb{R}^{n(K-1)+Kd}$ , the log-likelihood is defined as

$$\begin{aligned} \log p(\xi_i | Z^{(n)}) &\propto \sum_{k=1}^K \left[ -\frac{1}{2\sigma^2} (\xi_{i,k}^{(2)} - m_0)^T (\xi_{i,k}^{(2)} - m_0) \right] - n \log K \\ &\quad + \sum_{j=1}^N \sum_{k=1}^K \mathbb{1}_{\{\xi_{i,j}^{(1)} = b_k\}} \left[ -\frac{1}{2\lambda^2} (Z_j - m_k)^T (Z_j - m_k) \right], \end{aligned}$$

where the indicator function can be approximated by the Softmax functions in the computation. Specifically, for each sample  $\xi_i$ , we have

$$\mathbb{1}_{\{\xi_{i,j}^{(1)} = b_k\}} \approx W_{i,j,k} := \frac{\exp\left(\gamma(\langle x_{i,j}^{(1)}, b_k \rangle + \phi_k(x_i^{(2)}))\right)}{\sum_{\ell \in [K]} \exp\left(\gamma(\langle X_{i,j}^{(1)}, b_\ell \rangle + \phi_\ell(x_i^{(2)}))\right)},$$

where  $\gamma$  is a positive tuning parameter.

The calculation of the middle term in the objective (13) is straightforward, and only requires the knowledge of the target posterior  $\pi_n$  up to a normalizing constant. For the term  $\det(J_{\tilde{T}}(\tau, x^{(2)}))$  in (13), we note that  $\tilde{T}$  does not change the first component  $\tau \in \mathcal{Y}_1$  of the input, so that

$$J_{\tilde{T}}(\tau, x^{(2)}) = \begin{pmatrix} I & 0 \\ 0 & \nabla^2 \phi_\tau(x^{(2)}) \end{pmatrix}.$$

Therefore, the determinant of the Jacobian matrix at  $(\tau_i, x_i^{(2)})$  can be simplified into

$$\det(J_{\tilde{T}}(\tau_i, x_i^{(2)})) = \det(\nabla^2 \phi_{\tau_i}(x_i^{(2)})).$$

## A.4 Computation Details for Simulation Studies in Section 5

**Configurations for Section 5.1** We follow the optimization procedure described in Section B. In particular, we first generate 512 samples from the target distribution and initialize our transport map by minimizing the Sinkhorn distance between the transported draws through our transport map and those from the target distribution. After that, we further optimize our transport map via (5). We choose flow length = 64 for NF-planar in the experiment and we apply the same initialization to the NF map for fair comparison. Lastly, we choose 500 location-scale component maps for TMC.

**Configurations for Section 5.2** For the nonlinear function  $\varphi$ , we use  $K = 32$  convex units with Softsign functions. Since the target distribution is simple, we skip the initialization step and initialize all parameters from standard Gaussian distributions. We set flow length = 32 for NF-planar, and we use TMC with 300 location-scale component maps.

**Configurations for Section 5.3** To construct our transport map, we first choose unit vectors in  $\mathbb{R}^3$  for each value of the latent variables, since the components are not ordered. For the convex functions in formula (12), we adopt the “mean-field” approximation in (16). Since the continuous parameters follow unimodal distribution, we choose  $M = 1$  and  $K_i = 32$  for all convex functions. In addition, we choose  $\kappa = \frac{1}{n}$  for transport map formula (12) as suggested in Section 4.2.

## B Algorithm Description

In this section, we describe the details of the optimization procedure for the transport map. Since the optimization problem (5) can be highly non-convex, e.g., when the density of the target distribution is not log-concave, a good initialization of the parameters in the transport map is critical to achieve good optimization performance. Therefore, our optimization of the transport map can be decomposed into two steps: (1) initializing the parameters by minimizing the Sinkhorn divergence; (2) further optimizing the parameters by minimizing the KL-divergence. We employ the stochastic gradient-based optimization methods to optimize the parameters in the transport map.

**Initialization.** We first generate  $N$  samples  $\{y_1, y_2, \dots, y_N\}$  i.i.d. from the target distribution. If directly sampling from the target distribution is not possible, we can apply approximation methods such as MCMC or variational inference to obtain approximate draws of the target distribution. Since our goal is only to find good initialization of parameters, it is not required to have the approximation draws with high accuracy. After obtaining  $N$  draws from the target distribution, we will minimize the distance between the transported points  $\{T(x_1), T(x_2), \dots, T(x_N)\}$  from the reference distribution through map  $T$  and  $\{y_1, y_2, \dots, y_N\}$  to optimize the parameters in the transport map  $T$

$$\hat{T}_{\text{init}} = \arg \min_{T \in \mathfrak{T}} d(\{T(x_i)\}_{i=1}^n, \{y_i\}_{i=1}^n)$$

with the distance function  $d(\cdot, \cdot)$  being Sinkhorn distance (Cuturi, 2013) or Wasserstein GAN distance (Arjovsky et al., 2017). In our implementation, we use the Python Optimal Transport (Flamary et al., 2021) framework to compute the Sinkhorn distance and ADAM optimizer (Kingma and Ba, 2014) for gradient descent.

**Optimization.** Since the optimization programs for continuous and mixed variables cases are similar, except for the approximated conditional probability in (13) (see Section A.2), we focus on the continuous variables case here for conciseness.

In order to fit into the more general case where the number of the discontinuous regions in the target distribution is not known or the target distribution is multimodal, we construct the approximate family of transport map through the maximum of convex functions as in (11).

$$\mathfrak{T} := \left\{ T = \nabla u \mid u(x) = \max_{k \in [L]} u_k(x), u_k(x) = \sum_{m=1}^M f(x; \alpha_m^{(k)}, \beta_m^{(k)}, w_m^{(k)}, v_m^{(k)}), \right. \\ \left. \alpha_m^{(k)} \in \mathbb{R}^p, \beta_m^{(k)} \in \mathbb{R}^p, w_m^{(k)} \in \mathbb{R}, v_m^{(k)} \in \mathbb{R}, \text{ for all } k \in [L] \text{ and } m \in [M] \right\}. \quad (21)$$

Starting from the initialized parameter values obtained in the previous step, we apply stochastic gradient-based methods to solve the optimization problem in (5). In each iteration, the estimated objective function and its gradient with respect to the parameters  $\gamma := (\alpha_m^{(k)}, \beta_m^{(k)}, w_m^{(k)}, v_m^{(k)})$  are obtained through Monte Carlo method. We first generate  $N$  samples  $\{x_1, x_2, \dots, x_N\}$  i.i.d. from

the reference distribution  $\mu$ . The estimated objective function and its gradient are defined as

$$\begin{aligned}\widehat{d}_{\text{KL}} &:= \frac{1}{N} \sum_{i=1}^N [\log(\pi_n \circ T(x_i)) + \log |\det(J_T(x_i))|] \\ \widehat{\Gamma}_t(\boldsymbol{\gamma}) &:= \frac{1}{N} \sum_{i=1}^N [\nabla_{\boldsymbol{\gamma}} \log(\pi_n \circ T(x_i)) + \nabla_{\boldsymbol{\gamma}} \log |\det(J_T(x_i))|],\end{aligned}$$

and the parameters are updated through

$$\boldsymbol{\gamma}_{t+1} \leftarrow \boldsymbol{\gamma}_t + \eta_t \widehat{\Gamma}_t(\boldsymbol{\gamma}_t),$$

where  $\eta_t$  is the learning rate and can be updated based on ADAM optimizer (Kingma and Ba, 2014).

We use the PyTorch auto-differentiation to obtain estimated gradient  $\widehat{\Gamma}_t(\boldsymbol{\gamma})$ , which requires the objective function to be differential with respect to the parameters. To make  $\widehat{d}_{\text{KL}}$  differentiable, we approximate the max function in (21) with Softmax function, i.e.,

$$\begin{aligned}T(x) &\approx \sum_{k=1}^L \omega_k(x) \nabla u_k(x) \\ J_T(x) &\approx \sum_{k=1}^L \omega_k(x) \nabla^2 u_k(x)\end{aligned}$$

with

$$\omega_k(x) = \frac{\exp(\gamma u_k(x))}{\sum_{l \in [L]} \exp(\gamma u_l(x))},$$

where  $\gamma > 0$  is the concentration parameter. When  $\gamma$  goes to infinity, only one  $\omega_k$  are close to one while all other  $\omega_k$ 's will be close to zero. As a result, the Softmax approximation will be close to the maximum function when  $\gamma \rightarrow \infty$ .

For the stopping criteria, we will stop the optimization when the empirical objective  $\widehat{d}_{\text{KL}}$  does not improve within a number of iterations. Alternatively, we can consider a quantitative method used in El Moselhy and Marzouk (2012), where they use the empirical variance of the objective function

(5) over reference samples  $\{x_1, x_2, \dots, x_N\}$  to monitor the convergence. When the pushforward distribution  $T_{\#}\mu$  is close to  $\pi_n$ , the empirical variance is close to zero. Therefore, we can stop the optimization when the empirical variance falls below some positive threshold.

## C Proofs

In this section, we collect proofs to the main theoretical results presented in the main paper.

### C.1 Lemma from Panov and Spokoiny (2015)

We summarize the result from Panov and Spokoiny (2015) below which is a key ingredient of our proof.

**Lemma 8.** *Suppose function  $f \in \mathbb{R}^p$  is closed, strictly convex and differentiable. Let  $f^\dagger \in \mathbb{R}^p$  denote the conjugate function of  $f$ . Then,*

$$(\nabla f^\dagger)^{-1}(x) = \nabla f(x).$$

*Proof.* : Since function  $f$  is closed and strictly convex, the conjugate function of  $f^\dagger$  is still  $f$ . Therefore, for any  $x \in \mathbb{R}^p$ , we have

$$f(x) = \sup_{z \in \mathbb{R}^p} \{\langle x, z \rangle - f^\dagger(z)\}.$$

Suppose the above optimization problem is maximized at  $y \in \mathbb{R}^p$ , then we have

$$\nabla_y [\langle x, y \rangle - f^\dagger(y)] = 0 \implies \nabla f^\dagger(y) = x \implies y = (\nabla f^\dagger)^{-1}(x),$$

and

$$f(x) = \langle x, y \rangle - f^\dagger(y). \tag{22}$$

By the definition of the conjugate function  $f^*$ , we have

$$f^\dagger(y) = \sup_{z \in \mathbb{R}^p} \{\langle y, z \rangle - f(z)\}.$$

Then, according to the equation (22), the above optimization problem is maximized at point  $x$ . Therefore, we have

$$\nabla_x [\langle y, x \rangle - f(x)] = 0 \implies \nabla f(x) = y.$$

Combined with the above equation, it can be shown that

$$y = \nabla f(x) = (\nabla f^\dagger)^{-1}(x).$$

□

## C.2 Proof of Lemma 1

We first consider the case where  $\mu$  and  $\pi_n$  are continuous, and slightly abuse the same notation for their corresponding density function

$$\begin{aligned} d_{\text{KL}}(T_{\#}\mu \parallel \pi_n) &\equiv \int \mu(T^{-1}(\theta)) |\det J_{T^{-1}}(\theta)| \log \frac{\mu(T^{-1}(\theta)) |\det J_{T^{-1}}(\theta)|}{\pi_n(\theta)} d\theta \\ &= \int \mu(\xi) \log \frac{\mu(\xi) |\det J_T(\xi)|^{-1}}{\pi_n(T(\xi))} d\xi \\ &= \mathbb{E}_\mu[-\log \pi_n \circ T - \log |\det(J_T)| + \log \mu]. \end{aligned} \tag{23}$$

Because the source distribution  $\mu$  is fixed throughout the training, the third term  $\mathbb{E}_\mu[\log \mu]$  is a constant term. Therefore, the optimization is equivalent to the minimization of the first two terms.

If one of the distribution is not continuous, we replace the underlying Lebesgue measure by the source measure  $\mu$ , and the ratio of density functions by the corresponding Radon-Nicodym derivative.

### C.3 Proof of Lemma 4

Since  $h(x) = \langle \alpha, x \rangle + w$  is a linear function over  $x \in \mathbb{R}^p$ , it is convex. Moreover, as  $\varphi$  is increasing and bounded, the function  $u \mapsto \int_0^u \varphi(s) ds$  is convex over  $u \in \mathbb{R}$ . As a result, the function  $f$  as compositions of convex function and linear function is also convex.

### C.4 Proof of Theorem 1

Our proof has two parts. In the first part, we show that any optimal transport map must take the form of formula (12). In the second part, we show that if any transport map  $T$  takes the form of (12) and pushforwards the reference measure  $\mu$  to the target posterior  $\pi_n$ , i.e.  $T_{\#}\mu = \pi_n$ , then it must be an optimal transport map from  $\mu$  to  $\pi_n$ . Finally, these two properties together with the uniqueness and regularity properties in Lemma 2 lead to the claimed results.

**Part 1: OT map must take (12).** In this part of the proof, we derive the optimal transport map between the reference distribution  $\mu$  and target distribution  $\pi_n$  which contains both discrete and continuous components. We define a random variable  $Y = (Y^{(1)}, Y^{(2)}) := (b_\tau, \zeta) \in \{b_k\}_{k=1}^K \times \mathbb{R}^p$  associated with  $\theta = (\tau, \zeta)$ . For notation simplicity, we also assume  $Y$  to follow  $\pi_n$ .

The Kantorovich problem between  $X \sim \mu$  and  $Y \sim \pi_n$  associated with the problem (MPm) is defined as

$$(K\text{Pm}) \quad \inf_{\gamma \in \Pi(\mu, \pi_n)} \int \kappa \|x^{(1)} - y^{(1)}\|^2 + \|x^{(2)} - y^{(2)}\|^2 d\gamma(x, y).$$

Then, the dual formulation for (K\text{Pm}), known as Kantorovich duality, is defined as

$$\begin{aligned} & \sup_{\varphi, \psi} \int_{\mathbb{R}^r \times \mathbb{R}^p} \varphi(x) d\mu(x) + \int_{\mathbb{R}^r \times \mathbb{R}^p} \psi(y) d\pi_n(y), & (24) \\ & \text{s.t. } \varphi \in L^1(\mu), \quad \psi \in L^1(\pi_n) \\ & \text{and } \varphi(x) + \psi(y) \leq \kappa \|x^{(1)} - y^{(1)}\|^2 + \|x^{(2)} - y^{(2)}\|^2 \\ & \text{for every } x \in \mathbb{R}^r \times \mathbb{R}^p \quad \text{and} \quad y \in \{b_k\}_{k=1}^K \times \mathbb{R}^p. \end{aligned}$$

For each eligible function pair  $(\varphi, \psi)$  in (24), we have

$$\begin{aligned} \varphi(x) + \psi(y) &\leq \kappa \|x^{(1)} - y^{(1)}\|^2 + \|x^{(2)} - y^{(2)}\|^2 \\ \iff \underbrace{\kappa \|x^{(1)}\|^2 + \|x^{(2)}\|^2 - \varphi(x)}_{f(x)} + \underbrace{\kappa \|y^{(1)}\|^2 + \|y^{(2)}\|^2 - \psi(y)}_{g(y)} \\ &\geq 2\kappa \langle x^{(1)}, y^{(1)} \rangle + 2 \langle x^{(2)}, y^{(2)} \rangle. \end{aligned}$$

Therefore, the dual formulation (24) can be equivalently written as

$$\begin{aligned} \text{(DPm)} \quad C_{\mu, \pi_n} - \inf_{f, g} &\left\{ \int_{\mathbb{R}^r \times \mathbb{R}^p} f(x) \, d\mu(x) + \int_{\mathbb{R}^r \times \mathbb{R}^p} g(y) \, d\pi_n(Y) \right\}, \\ \text{s.t.} \quad &f \in L^1(\mu), \quad g \in L^1(\pi_n) \\ &\text{and } f(x) + g(y) \geq 2\kappa \langle x^{(1)}, y^{(1)} \rangle + 2 \langle x^{(2)}, y^{(2)} \rangle \\ &\text{for every } x \in \mathbb{R}^r \times \mathbb{R}^p \quad \text{and } y \in \{b_k\}_{k=1}^K \times \mathbb{R}^p, \end{aligned}$$

where

$$C_{\mu, \pi_n} := \int_{\mathbb{R}^r \times \mathbb{R}^p} \kappa \|x^{(1)}\|^2 + \|x^{(2)}\|^2 \, d\mu(x) + \int_{\mathbb{R}^r \times \mathbb{R}^p} \kappa \|y^{(1)}\|^2 + \|y^{(2)}\|^2 \, d\pi_n(y).$$

Therefore, for any eligible pair of functions  $(f, g)$  in problem (DPm), we have

$$\begin{aligned} f(x) &\geq \sup_{z \in \{b_k\}_{k=1}^K \times \mathbb{R}^p} \left\{ 2\kappa \langle x^{(1)}, z^{(1)} \rangle + 2 \langle x^{(2)}, z^{(2)} \rangle - g(z) \right\} \\ &= 2 \sup_{k \in [K]} \left\{ \kappa \langle x^{(1)}, b_k \rangle + \sup_{z^{(2)} \in \mathbb{R}^p} \left\{ \langle x^{(2)}, z^{(2)} \rangle - \frac{1}{2} g(z^{(1)}, z^{(2)}) \right\} \right\}. \end{aligned} \quad (25)$$

We define  $h(y) := \frac{1}{2}g(y)$  over  $\{b_k\}_{k=1}^K \times \mathbb{R}^p$  and  $h_k(y^{(2)}) := h(b_k, y^{(2)})$  for  $k \in [K]$ . Then, for any function pair  $(f, h)$  eligible for problem (DPm), we have

$$f(x) + 2h(y) \geq 2\kappa \langle x^{(1)}, y^{(1)} \rangle + 2 \langle x^{(2)}, y^{(2)} \rangle.$$

In the following, we show that it suffices to only consider convex functions for  $h_k$  to solve the

problem (DPM). For any function  $h_k$  in  $\mathbb{R}^p$ , its convex conjugate function is defined as

$$h_k^*(x^{(2)}) := \sup_{Z^{(2)} \in \mathbb{R}^p} \{ \langle x^{(2)}, Z^{(2)} \rangle - h_k(Z^{(2)}) \}.$$

Then, we define a function  $\tilde{f}$  over  $\mathbb{R}^r$  as

$$\begin{aligned} \tilde{f}(x) &:= 2 \sup_{k \in [K]} \{ \kappa \langle x^{(1)}, b_k \rangle + h_k^*(x^{(2)}) \} \\ &= 2 \sup_{k \in [K]} \left\{ \kappa \langle x^{(1)}, b_k \rangle + \sup_{z^{(2)} \in \mathbb{R}^p} \{ \langle x^{(2)}, Z^{(2)} \rangle - h_k(Z^{(2)}) \} \right\}. \end{aligned} \quad (26)$$

For any function pair  $(f, h)$  eligible for problem (DPM), the pair  $(\tilde{f}, h)$  improves the value of the objective function in (DPM), since  $f(x) \geq \tilde{f}(x)$  for all  $x \in \mathbb{R}^r$  according to the definition of  $\tilde{f}$  and the inequality in (25). Then, we can define a function  $h_k^\dagger$  over  $\mathbb{R}^p$  as the convex conjugate function of  $h_k^*$  and function  $h^\dagger(b_k, y^{(2)}) := h_k^\dagger(y^{(2)})$  over  $\{b_k\}_{k=1}^K \times \mathbb{R}^p$ . The function pair  $(\tilde{f}, h^\dagger)$  will further improve  $(\tilde{f}, h)$  on the value of the objective function in (DPM), since  $h(y) \geq h^\dagger(y)$  for all  $y = (b_k, y^{(2)}) \in \{b_k\}_{k=1}^K \times \mathbb{R}^p$  by the definition of the conjugate functions, i.e.,

$$\begin{aligned} h^\dagger(y) &= h_k^\dagger(y^{(2)}) \\ &= \sup_{x^{(2)} \in \mathbb{R}^p} \{ \langle x^{(2)}, y^{(2)} \rangle - h_k^*(x^{(2)}) \} \\ &= \sup_{x^{(2)} \in \mathbb{R}^p} \left\{ \langle x^{(2)}, y^{(2)} \rangle - \sup_{Z^{(2)} \in \mathbb{R}^p} \{ \langle x^{(2)}, Z^{(2)} \rangle - h_k(Z^{(2)}) \} \right\} \\ &\leq \sup_{x^{(2)} \in \mathbb{R}^p} \{ \langle x^{(2)}, y^{(2)} \rangle - \langle x^{(2)}, y^{(2)} \rangle + h_k(y^{(2)}) \} \\ &= h_k(y^{(2)}) = h(y). \end{aligned}$$

Based on the above discussion, the problem (DPM) can be formulated as a problem with  $K$  convex functions  $h_k(y^{(2)})$  for  $k \in [K]$ , i.e.,

$$\begin{aligned} (\text{DPM}') \quad & C_{\mu, \pi_n} - 2 \cdot \inf_{f, h} \left\{ \int_{\mathbb{R}^r \times \mathbb{R}^p} f(x) d\mu(x) + \int_{\{b_k\}_{k=1}^K \times \mathbb{R}^p} h(y) d\pi_n(y) \right\}, \\ \text{s.t.} \quad & h \in L^1(\pi_n) \quad \text{and} \quad h_k(y^{(2)}) := h(b_k, y^{(2)}) \text{ is convex over } \mathbb{R}^p \text{ for } k \in [K] \end{aligned}$$

$$\text{and } f(x) := \max_{k \in [K]} \{ \kappa \langle x^{(1)}, b_k \rangle + h_k^*(x^{(2)}) \}.$$

According to the duality equality between (KPm) and (DPm) and the equivalence between (DPm) and (DPm'), it is satisfied that if point  $(x, y)$  belongs to the support of the optimal transport plan  $\gamma$  between  $\mu$  and  $\pi_n$  minimizing (KPm) and  $(f, h)$  is a pair of functions maximizing (DPm'), then

$$f(x) + h(y) = \kappa \langle x^{(1)}, y^{(1)} \rangle + \langle x^{(2)}, y^{(2)} \rangle.$$

This implies that for  $(x, y) \in \gamma$  with  $y = (b_\tau, \zeta)$ , it satisfies

$$\begin{aligned} & \kappa \langle x^{(1)}, b_\tau \rangle + \langle x^{(2)}, \zeta \rangle - h_\tau(\zeta) \\ &= \max_{k \in [K]} \{ \kappa \langle x^{(1)}, b_k \rangle + h_k^*(x^{(2)}) \} \\ &= \max_{k \in [K]} \left\{ \kappa \langle x^{(1)}, b_k \rangle + \sup_{Z^{(2)} \in \mathbb{R}^p} \{ \langle x^{(2)}, Z^{(2)} \rangle - h_k(Z^{(2)}) \} \right\} \\ &\geq \{ \kappa \langle x^{(1)}, b_\tau \rangle + \langle x^{(2)}, \zeta \rangle - h_\tau(\zeta) \} \end{aligned} \tag{27}$$

where the first equation is by the definition of  $f$ . Therefore, the equality is achieved in the last step. According to equation (27), the discrete random variable  $\tau \in [K]$  associated with  $b_\tau$  is then defined as

$$\tau = \arg \max_{k \in [K]} \{ \kappa \langle x^{(1)}, b_k \rangle + h_k^*(x^{(2)}) \}.$$

Then, by plugging the definition of  $\tau$  into (27), we have

$$h_\tau^*(x^{(2)}) = \langle x^{(2)}, \zeta \rangle - h_\tau(\zeta).$$

According to the definition of the conjugate function  $h_\tau^*$  of  $h_\tau$ , the following equation is satisfied.

$$\nabla_\zeta [\langle x^{(2)}, \zeta \rangle - h_\tau(\zeta)] = 0 \implies x^{(2)} - \nabla h_\tau(\zeta) = 0.$$

Therefore, we have

$$\zeta = (\nabla h_\tau)^{-1}(x^{(2)}) = \nabla h_\tau^*(x^{(2)}),$$

where the second equality is according to Lemma 8.

Based on the above relationship between the optimal transport plan  $\gamma$  solving (KPM) and the function pair  $(f, h)$  solving (DPM'), the optimal transport map  $T^*$  that pushforwards  $\mu$  to  $\pi_n$  can be characterized through  $K$  convex functions  $\{\phi_k\}_{k=1}^K$  over  $\mathbb{R}^p$  with  $\phi_k(x^{(2)}) := \frac{1}{\kappa} h_k^*(x^{(2)})$  for  $k \in [K]$ . Specifically,  $T^*$  maps  $(x^{(1)}, x^{(2)})$  to  $(\tau, \zeta)$  with

$$\begin{cases} \tau = T^{*(1)}(x^{(1)}, x^{(2)}) = \arg \max_{k \in [K]} \{ \langle x^{(1)}, b_k \rangle + \phi_k(x^{(2)}) \}, \\ \zeta = T^{*(2)}(x^{(1)}, x^{(2)}) = \kappa \nabla \phi_\tau(x^{(2)}). \end{cases} \quad (28)$$

In addition, the convex function  $u^*$  associated with the optimal transport map  $T^*$  is in form of function  $f$ , i.e.,

$$u^*(x^{(1)}, x^{(2)}) = \kappa \max_{k \in [K]} \{ \langle x^{(1)}, b_k \rangle + \phi_k(x^{(2)}) \}.$$

**Part 2: Map with Form (12) is Optimal.** In this part of the proof, we show the following property: suppose there exists a transport map  $T_0$  in form of (28) satisfying  $(T_0)_\#(\mu) = \pi_n$ , the transport map  $T_0$  is then the optimal transport map for the problem (MPM). In addition, the induced transport plan  $(id, T_0)_\#(\mu)$  is the optimal plan for the Kantorovich problem (KPM) between  $\mu$  and  $\pi_n = (T_0)_\#(\mu)$ .

To see this, suppose there exist convex functions  $\{\phi_k\}_{k=1}^K$  such that  $(T_0)_\#(\mu) = \pi_n$ . We can define a pair of  $(f, h)$  that is eligible for problem (DPM'), i.e.,

$$f(x^{(1)}, x^{(2)}) := \kappa \max_{k \in [K]} \{ \langle x^{(1)}, b_k \rangle + \phi_k(x^{(2)}) \}$$

$$h(b_\tau, \zeta) := (\kappa \phi_\tau)^*(\zeta) \quad \text{for } \tau \in [K],$$

where  $(\kappa \phi_k)^*$  is the convex conjugate function of  $\kappa \phi_k$  for  $k \in [K]$ .

For any point  $(x, y)$  with  $y = (b_\tau, \zeta)$  that belongs to the support  $\gamma_0 = (id, T_0)_\#(\mu)$ , we have

$$\begin{aligned} f(x) + h(y) &= \max_{k \in [K]} \kappa \{ \langle x^{(1)}, b_k \rangle + \phi_k(x^{(2)}) \} + (\kappa\phi_\tau)^*(\zeta) \\ &= \kappa \langle x^{(1)}, b_\tau \rangle + \kappa\phi_\tau(x^{(2)}) + (\kappa\phi_\tau)^*(\zeta) \\ &= \kappa \langle x^{(1)}, b_\tau \rangle + \langle x^{(2)}, \zeta \rangle, \end{aligned}$$

where the second equation is by the definition of  $\tau$  in (28) and the third equation is by the property of the convex function  $\kappa\phi_\tau$ .

Therefore, we have the following inequality.

$$\begin{aligned} \min(\text{KPM}) &\leq \int \kappa \|x^{(1)} - y^{(1)}\|^2 + \|x^{(2)} - y^{(2)}\|^2 d\gamma_0(x, y) \\ &= C_{\mu, \pi_n} - 2 \int \kappa \langle x^{(1)}, y^{(1)} \rangle + \langle x^{(2)}, y^{(2)} \rangle d\gamma_0(x, y) \\ &= C_{\mu, \pi_n} - 2 \int f(x) + h(y) d\gamma_0(x, y) \\ &= C_{\mu, \pi_n} - 2 \left[ \int f(x) d\mu(x) + \int h(x) d\pi_n(y) \right] \\ &\leq \max(\text{DPM}'). \end{aligned}$$

In addition, since  $\min(\text{KPM}) \geq \max(\text{DPM}')$  by the inequality between the primal and dual problems, we have  $\min(\text{KPM}) = \max(\text{DPM}')$ . Therefore  $T_0$  is the optimal transport map that pushforwards  $\mu$  to  $\pi_n$  and  $(id, T_0)_\#(\mu)$  is the optimal plan between  $\mu$  and  $\pi_n = (T_0)_\#(\mu)$ .

## C.5 Proof of Lemma 6

Let us denote the intermediate joint density of  $(\tau, X^{(2)})$  as  $\tilde{\nu}(\tau, X^{(2)}) := P(\tau | X^{(2)})\mu_2(X_2)$ . Then we can rewrite the KL divergence in (4) as

$$\begin{aligned} d_{\text{KL}}(T_\# \mu | | \pi_n) &= \int \tilde{\nu}(\tilde{T}^{-1}(\tau, \zeta)) \left| \det J_{\tilde{T}^{-1}}(\tau, \zeta) \right| \log \frac{\tilde{\nu}(\tilde{T}^{-1}(\tau, \zeta)) \left| \det J_{\tilde{T}^{-1}}(\tau, \zeta) \right|}{\pi_n(\tau, \zeta)} d\tau d\zeta \\ &= \int \tilde{\nu}(\tau, X^{(2)}) \log \frac{\tilde{\nu}(\tau, X^{(2)}) \left| \det J_{\tilde{T}}(\tau, X^{(2)}) \right|^{-1}}{\pi_n(\tilde{T}(\tau, X^{(2)}))} d\tau dX^{(2)} \end{aligned}$$

$$\begin{aligned}
&= \int \tilde{\nu}(\tau, X^{(2)}) \log \frac{P(\tau | X^{(2)}) \mu_2(X^{(2)}) |\det J_{\tilde{T}}(\tau, X^{(2)})|^{-1}}{\pi_n(\tilde{T}(\tau, X^{(2)}))} d\tau dX^{(2)} \\
&= \int \sum_{k=1}^K P(k | X^{(2)}) \mu_2(X^{(2)}) \log \frac{P(k | X^{(2)}) \mu_2(X^{(2)}) |\det J_{\tilde{T}}(k, X^{(2)})|^{-1}}{\pi_n(\tilde{T}(k, X^{(2)}))} dX^{(2)}.
\end{aligned}$$

Since we know given  $X^{(1)}, X^{(2)}$ ,  $\tau$  is deterministic (we abuse the notation as  $\tau(X^{(1)}, X^{(2)})$ )

$$P(k | X^{(2)}) = \int P(k | X^{(1)}, X^{(2)}) \mu(X^{(1)} | X^{(2)}) dX^{(1)} = \int 1_{\tau(X^{(1)}, X^{(2)})=k} \mu(X^{(1)} | X^{(2)}) dX^{(1)},$$

then we can proceed the KL divergence derivation as

$$\begin{aligned}
d_{\text{KL}}(T_{\#}\mu || \pi_n) &= \int \sum_{k=1}^K 1_{\tau(X^{(1)}, X^{(2)})=k} \mu(X) \log \frac{P(k | X^{(2)}) \mu_2(X^{(2)}) |\det J_{\tilde{T}}(k, X^{(2)})|^{-1}}{\pi_n(\tilde{T}(k, X^{(2)}))} dX^{(1)} dX^{(2)} \\
&= \int \mu(X) \log \frac{P(\tau | X^{(2)}) \mu_2(X^{(2)}) |\det J_{\tilde{T}}(\tau, X^{(2)})|^{-1}}{\pi_n(\tilde{T}(\tau, X^{(2)}))} dX^{(1)} dX^{(2)} \\
&= \int \mu(X) \log \frac{P(\tau | X^{(2)}) |\det J_{\tilde{T}}(\tau, X^{(2)})|^{-1}}{\pi_n(\tilde{T}(\tau, X^{(2)}))} dX^{(1)} dX^{(2)} + \text{const.}
\end{aligned}$$